IEEE Access
Multidisciplinary ⋮ Rapid Review ⋮ Open Access Journal

Received 30 May 2026, accepted 15 June 2026, date of publication 18 June 2026, date of current version 24 June 2026.

Digital Object Identifier 10.1109/ACCESS.2026.3705316

RESEARCH ARTICLE

Complexity Reduction in RIS Optimization: A User Grouping and Adaptive Beamforming Approach

MUTEEN MUNAWAR, (Student Member, IEEE), MAMOUN GUENACH, (Senior Member, IEEE), AND INGRID MOERMAN, (Fellow, IEEE)

Interuniversity Microelectronics Centre (IMEC), 3000 Leuven, Belgium
IDLab, Ghent University, 9000 Ghent, Belgium

Corresponding author: Muteen Munawar (muteen.munawar@imec.be)

This work was supported in part by European Community's Research Foundation Flanders (FWO) under Grant A2582000101, and in part by the Project Strip-Link multiple-input multiple-output (MIMO) through FWO under Grant 97707.

ABSTRACT This paper addresses a critical challenge of high computational complexity in the optimization of reconfigurable intelligent surfaces (RISs), a bottleneck that currently prevents real-time implementation in practical wireless networks. Existing iterative algorithms often exceed the channel coherence time, necessitating a shift toward insight-driven, low-complexity solutions. Specifically, we observe that the multiplicative fading nature of passive RISs means their impact is localized; thus, users strongly dominated by the direct transmit source receive negligible gains from RIS optimization. Based on this, we propose a novel User Grouping (UG) framework that categorizes users into three or two groups (3-UG and 2-UG) according to their relative direct and reflected channel strengths. By optimizing RIS operations only for relevant user subsets, we significantly limit the number of computational constraints. Furthermore, we investigate a per-user multi-stream transmission problem involving mixed-integer log-sum expressions. We derive a geometric-mean (GM)-based convex formulation to handle these discrete variables and develop a multi-step alternating optimization (AO) algorithm. Finally, we extend the UG concept to point-to-point (P2P) multiple-input multiple-output (MIMO) by introducing Adaptive Selection Beamforming (ASB), a non-iterative method that selects between two low-complexity solution sets. Numerical results demonstrate that the proposed UG methods achieve up to a 77% reduction in computational complexity compared to traditional benchmarks. Additionally, the non-iterative ASB-MIMO scheme is found to be approximately 67%–85% less complex (depending on the MIMO size) than the most efficient existing closed-form solutions. In all scenarios, the proposed frameworks maintain near-optimal performance with negligible performance degradation.

INDEX TERMS Reconfigurable intelligent surfaces, low complexity, multiuser, multi-stream transmission, user grouping, adaptive selection beamforming, alternating optimization.

I. INTRODUCTION

The concept of a reflecting surface with multiple reflecting elements having fixed phases is not new in the literature [1]. However, recent advances in metamaterial literature have enabled real-time control of metamaterial properties, opening up new opportunities for metasurfaces in wireless communications [2]. For example, a metasurface-based reconfigurable intelligent surface (RIS) [3] provides real-time amplitude and phase changes to the incident signal, as well as polarization conversion [4], [5] and energy split [6], [7], [8], offering potential applications such as improved signal-to-noise ratio (SNR) [9], enhanced coverage [10], increased security [11], reduced interference [12], and reflected modulation [13], [14]. Corresponding to these applications, extensive literature exists on beamforming [15], [16] and channel estimation methods [17], [18] for these metasurfaces.

To get benefits out of RIS, optimizing its elements is an important step. Hence, the literature contains several studies where RIS elements have been optimized to achieve

The associate editor coordinating the review of this manuscript and approving it for publication was Cesar Vargas-Rosales.

© 2026 The Authors. This work is licensed under a Creative Commons Attribution 4.0 License.
For more information, see https://creativecommons.org/licenses/by/4.0/

various objectives. For instance, [2], [19] propose optimizing elements of RIS with the objective of maximizing signal strength at the user. Reference [9] proposes optimizing RIS to improve the rank of multiple-input multiple-output (MIMO) channels. Reference [20] studies RIS optimization to provide a uniform performance among users. Reference [13] optimizes RIS to implement passive modulation. References [4], [5] propose optimizing RIS to enhance interlayer multiplexing gains. Reference [21] proposes optimizing RIS elements to enhance communication as well as sensing performance.

All these studies optimize the operations of RISs with respect to several objective functions based on common methods like semidefinite relaxation (SDR) [22], manifold optimization [23], gradient descent [24], and successive convex approximations [25] for continuous variables. In contrast, tabu search [26], sphere decoder [27], and a family of metaheuristic optimization algorithms such as particle swarm optimization, simulated annealing, and differential evolution are also reported for discrete variables. Some special scenarios of RIS-assisted communication setups, such as single-user MISO and single-user MIMO, also allow for closed-form optimal solutions [19], [28], [29].

While these optimization techniques provide a theoretical foundation for RIS-assisted systems, their practical implementation is hindered by several hardware-level challenges. First, phase errors arising from hardware impairments and inaccurate control circuits can significantly degrade expected beamforming gains. Second, the element configuration of the surface, specifically the spatial arrangement and scaling to hundreds or thousands of elements, increases the search space and computational burden exponentially. Finally, to maintain a manageable overhead on the control link, phase shift compression (or quantization) is often required, where continuous phase shifts are mapped to a limited set of discrete levels [12].

These constraints, coupled with the computationally expensive iterative nature of standard algorithms like SDR and manifold optimization, result in a critical real-time feasibility gap. In practical communication scenarios, the optimization of hundreds of RIS elements must occur within the channel coherence time; however, current iterative approaches often fail to meet this requirement [16]. This is primarily why a general-purpose prototype of an RIS-assisted wireless network with real-time optimization has not yet been possible, despite specialized prototypes for passive modulation [30] or fixed user positions [31]. Our motivation in this work stems from bridging this gap by exploiting the "multiplicative fading" effect inherent to passive RISs. By identifying and grouping users who truly benefit from the reflected path versus those dominated by the direct link, we can bypass unnecessary computations. This work aims to shift the paradigm toward a low-complexity, insight-driven framework that can help make real-time RIS applications a reality.

In this context, the main contributions of this paper are summarized as follows:

1) **A Novel User Grouping (UG) Framework:** We observe that the impact of the RIS is localized due to multiplicative fading; thus, users strongly influenced by the direct source receive negligible gains from RIS optimization. We propose a framework that categorizes users (Groups A, B, and C) to selectively optimize RIS phases. Importantly, this is a generalized framework applicable to existing algorithms and various architectures, including STAR-RIS [32] and omni-RIS [33].
2) **A Non-Iterative ASB-MIMO Scheme:** We extend the UG concept to P2P MIMO scenarios. While current low-complexity solutions [4], [29] remain iterative and are only optimal for low-SNR regimes, we propose an **Adaptive Selection Beamforming (ASB)** method. Our approach is entirely **non-iterative**, selecting between two optimal candidate solution sets to achieve near-optimal performance with significantly reduced computational burden.
3) **Mixed-Integer Multi-Stream Optimization:** We introduce a generalized multiuser, multi-stream MIMO system model involving mixed-integer log-sum expressions coupled with discrete stream variables. To solve this challenge, which is currently unaddressed in the literature, we propose a **geometric-mean (GM)-based convex formulation** and derive a multi-step alternating optimization (AO) algorithm that serves as a high-performance benchmark for our proposed strategies.
4) **Comprehensive Complexity and Performance Analysis:** We provide an exhaustive numerical analysis and a detailed computational complexity analysis, i.e., CPU time and floating-point operations (FLOPs), demonstrating that our methods reduce complexity by up to 77% with negligible performance degradation, thereby facilitating future studies on real-time RIS deployment.

The remainder of this paper is organized as follows. Section II presents the system model and formulates the problem. In Section III, we derive convex solutions and propose algorithms based on standard methods. Section IV proposes the UG method for the multiuser case, whereas Section V introduces a low-complexity solution for the P2P MIMO system. Sections VI and VII present the numerical analysis for the multiuser and the P2P MIMO scenarios, respectively. Section VIII provides the analytical computational complexity analysis. Section IX presents a discussion of related extensions and the selection of the grouping threshold. Finally, Section X concludes the paper.

Notations: Scalars are denoted by italic letters, whereas vectors and matrices are denoted by bold-face lower- and upper-case letters, respectively. For a complex-valued vector v of length N, v^T denotes the transpose, $v_{(n)}$ denotes the n-th element of v, v^* denotes the complex conjugate

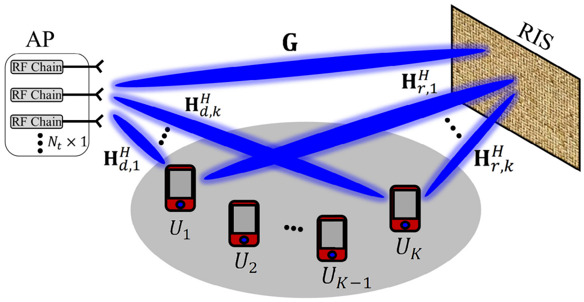

FIGURE 1. RIS-assisted multiuser multi-stream MIMO.

of each element, 1_v denotes a vector of size v with all entries 1, v^H denotes the conjugate transpose, $\|v\|$ denotes the Euclidean norm, diag (v) denotes a diagonal matrix with each diagonal element being the corresponding element in v, $v > 0$ denotes the number of non-zero elements in $\mathbf{v}$, log-sum (v) means $\sum_{k=1}^{K} \log(v_k)$, sum (v) means $\sum_{k=1}^{K}(v_k)$, and GM (v) represents the geometric mean. For a complex-valued matrix M, rank (M) denotes the rank, $M_{(n,m)}$ denotes the n-th row and m-th column entry, $M \succeq 0$ denotes that M is positive semi-definite (while $M \succ 0$ would denote positive definite), and trace (M) denotes trace. For a complex-valued square matrix A, I_A denotes an identity matrix of size A and A^{-1} denotes the inverse. The notation $(\cdot)^*$ denotes the complex conjugate of a complex number, $\underset{\max}{\hat{e}}(A, B)$ denotes the dominant generalized eigenvector of matrix pair (A, B).

II. SYSTEM MODEL AND PROBLEM FORMULATION

We consider a general multiuser MIMO setup, illustrated in Fig. 1, where an access point (AP) equipped with N_t antennas communicates with K users, each equipped with $N_{r,k}$ antennas, capable of receiving up to L_k data streams. The communication is assisted by an RIS comprising N passive reflecting elements. The total number of transmitted data streams in the system is given by $L = \sum_{k=1}^{K} L_k$, where $k = 1, \ldots, K$. The received signal at user k, after digital combining and RIS reflection, is expressed as:

$$y_k = \left(F_k H_{r,k}^H \Phi G + F_k H_{d,k}^H\right) \sum_{j=1}^{K} \sum_{l=1}^{L_j} w_{l,j} s_{l,j} + F_k z_k, \quad (1)$$

where $y_k \in \mathbb{C}^{L_k \times 1}$ denotes the post-processed received signal for user k, $F_k \in \mathbb{C}^{L_k \times N_{r,k}}$ is the digital receive filter, and z_k is the additive noise vector. The term $w_{l,j} \in \mathbb{C}^{N_t \times 1}$ represents the transmit digital filter used for the l-th stream of user j, $s_{l,j}$ is the corresponding data symbol, and Φ contains the RIS operations on its diagonal, i.e., diag $\left(e^{-j\phi_1}, \ldots, e^{-j\phi_N}\right)$. The composite channels are defined as follows: $G \in \mathbb{C}^{N \times N_t}$ for the AP-to-RIS link, $H_{r,k}^H \in \mathbb{C}^{N_{r,k} \times N}$ for the RIS-to-user-k link, and $H_{d,k}^H \in \mathbb{C}^{N_{r,k} \times N_t}$ for the direct AP-to-user-k link.[1]

[1]The discussion on the acquisition of channel state information is not within the scope of this work; it can be acquired using existing conventional schemes [34], [35], [36].

Let $H_k^H = \left(H_{r,k}^H \Phi G + H_{d,k}^H\right)$ denote the composite MIMO channel between the AP and user k. Then, the spectral efficiency (SE) for user k, achieved through L_k data streams, is denoted by c_k in (2), as shown at the bottom of the next page. where $\mathbf{f}_{k,l} \in \mathbb{C}^{N_{r,k} \times 1}$ represents the receive digital filter for the l-th data stream of user k, and the combined receive filter matrix for user k is given by $F_k^H = \left[f_{k,1}, f_{k,2}, \cdots, f_{k,L_k}\right]$.

In the context of multi-stream multiuser MIMO, we aim to determine the optimal number of data streams for all users, i.e., $L_k, \forall k$, which can ensure a target SE performance for all users, i.e., $\lambda_k, \forall k$, in the minimum possible transmit power at the AP. To achieve this goal, we need to optimize the transmit filter $w_{k,l}, \forall k, l$, receive filters $F_k, \forall k$, number of data streams $L_k, \forall k$, power allocations $p_k, \forall k$, and RIS operations Φ. Hence, the problem can be formulated as (P1), where, as mentioned earlier, λ_k represents the minimum SE requirement for user k, $P_{\max}$ denotes the maximum transmit power available at the AP, and p_k denotes the transmit power allocated to L_k data streams of user k, with $p_{k,l}$ being the power allocated to the l-th stream of user k such that $\sum_{l=1}^{L_k} p_{k,l} = p_k$.

The system model in Fig. 1 is well studied in the literature for several objectives, except that here we consider L_k as an optimization variable (discrete), which results in a mixed-integer optimization problem. Specifically, the objective and constraint 1 in problem (P1) are coupled with L_k.

Before we move to Sections IV and V, we show in Section III that existing algorithms are not applicable to (P1) owing to the log-sum expressions coupled with L_k. Nevertheless, the solutions we devise in Section III to solve (P1) are considered as benchmark schemes for the methods proposed in Sections IV and V.

$$\begin{aligned}
\min_{\mathbf{w}_{k,l}, \mathbf{f}_{k,l}, L_k, p_{k,l}, \Phi} \quad & \sum_{k=1}^{K} \sum_{l=1}^{L_k} p_{k,l} \\
\text{s.t.} \quad & c_k \geq \lambda_k, \quad \forall k, \\
& \mathbf{H}_k^H = \mathbf{H}_{r,k}^H \Phi \mathbf{G} + \mathbf{H}_{d,k}^H, \\
& \Phi = \mathrm{diag}\left(e^{-j\phi_1}, \ldots, e^{-j\phi_N}\right), \\
& \sum_{k=1}^{K} \sum_{l=1}^{L_k} p_{k,l} \leq P_{\max}.
\end{aligned} \quad \text{(P1)}$$

III. PROPOSED SOLUTION TO PROBLEM (P1)

A. OPTIMAL DESIGN OF TRANSMIT/RECEIVE DIGITAL FILTERS, NUMBER OF DATA STREAMS, AND POWER ALLOCATION

To address the joint mixed-integer optimization problem (P1), we adopt a decomposition-based alternating optimization strategy. We first decouple the digital variables from the RIS phases by fixing $\Phi = \mathbf{I}_\Phi$ (or a random matrix) for tractability. This results in the subproblem (P1.1), as shown at the bottom of the page, denoted as (P1.1), which aims to jointly determine the transmit/receive digital filters, optimal power allocations, and the number of data streams. Here $\|w_{k,l}\|^2 = p_{k,l}$. To solve the problem in (P1.1), we propose a four-step alternating optimization (AO) algorithm. We begin with an initial setting where the number of data streams per user, L_k, is set to $\min(N_t, N_{r,k})$, and the initial power allocation for each stream is $\frac{P_{\max}}{L_k}$. Based on this initialization, the transmit and receive filters, $\mathbf{w}_{k,l}$ and $\mathbf{f}_{k,l}$ for all k and l, are obtained using mutually dependent optimal linear minimum mean square error (MMSE) solutions:

$$\overline{\mathbf{w}}_{k,l} = \frac{\hat{\mathbf{e}}_{\max}\left(\mathbf{S}_{k,l}^{\mathbf{f}_{k,l}}, \ \mathbf{T}_{k,l}^{\mathbf{f}_{k,l}}\right)}{\left\|\hat{\mathbf{e}}_{\max}\left(\mathbf{S}_{k,l}^{\mathbf{f}_{k,l}}, \ \mathbf{T}_{k,l}^{\mathbf{f}_{k,l}}\right)\right\|} \tag{3}$$

$$\mathbf{f}_{k,l} = \frac{\hat{\mathbf{e}}_{\max}\left(\mathbf{S}_{k,l}^{\overline{\mathbf{w}}_{k,l}}, \ \mathbf{T}_{k,l}^{\overline{\mathbf{w}}_{k,l}}\right)}{\left\|\hat{\mathbf{e}}_{\max}\left(\mathbf{S}_{k,l}^{\overline{\mathbf{w}}_{k,l}}, \ \mathbf{T}_{k,l}^{\overline{\mathbf{w}}_{k,l}}\right)\right\|} \tag{4}$$

where

$$\mathbf{S}_{k,l}^{\mathbf{f}_{k,l}} = \mathbf{H}_k \mathbf{f}_{k,l} \mathbf{f}_{k,l}^H \mathbf{H}_k^H, \tag{5}$$

denotes the strength covariance matrix for the l-th stream of the k-th user when $\mathbf{f}_{k,l}$ is fixed.

$$\mathbf{S}_{k,l}^{\overline{\mathbf{w}}_{k,l}} = \mathbf{H}_k^H \overline{\mathbf{w}}_{k,l} \overline{\mathbf{w}}_{k,l}^H \mathbf{H}_k, \tag{6}$$

denotes the strength covariance matrix for the l-th stream of the k-th user when $\mathbf{w}_{k,l}$ is fixed. Whereas

$$\mathbf{T}_{k,l}^{\mathbf{f}_{k,l}} = \sum_{i\neq k}^{K}\sum_{m=1}^{L_i} p_{i,m}\mathbf{H}_i \mathbf{f}_{i,m}\mathbf{f}_{i,m}^H \mathbf{H}_i^H + \sum_{j\neq l}^{L_k} p_{k,j}\mathbf{H}_k \mathbf{f}_{k,j}\mathbf{f}_{k,j}^H \mathbf{H}_k^H + \sigma^2 \mathbf{I} \tag{7}$$

and

$$\mathbf{T}_{k,l}^{\overline{\mathbf{w}}_{k,l}} = \sum_{i\neq k}^{K}\sum_{m=1}^{L_i} p_{i,m}\mathbf{H}_k^H \overline{\mathbf{w}}_{i,m}\overline{\mathbf{w}}_{i,m}^H \mathbf{H}_k + \sum_{j\neq l}^{L_k} p_{k,j}\mathbf{H}_k^H \overline{\mathbf{w}}_{k,j}\overline{\mathbf{w}}_{k,j}^H \mathbf{H}_k + \sigma^2 \mathbf{I} \tag{8}$$

denote the interference-plus-noise strength covariance matrices for the l-th stream of the k-th user when $\mathbf{w}_{k,l}$ and $\mathbf{f}_{k,l}$ are fixed, respectively. Additionally, in (3)

$$\overline{\mathbf{w}}_{k,l} = \frac{\mathbf{w}_{k,l}}{\|\mathbf{w}_{k,l}\|}, \quad \forall k, l. \tag{9}$$

Upon obtaining the transmit and receive filters $\mathbf{w}_{k,l}$ and $\mathbf{f}_{k,l}$ for a given iteration, we fix these digital beamformers to further simplify the optimization landscape. By substituting these fixed filters into (P1.1) and defining the effective channel and interference terms $(a_{k,l}, b_{k,l}, e_{k,l})$, we derive subproblem (P1.2). This step allows us to specifically target the mixed-integer variables L_k and power levels $p_{k,l}$ for the convex approximation described in the following part.

$$\begin{aligned}
\min_{p_k} \quad & \sum_{k=1}^{K}\sum_{l=1}^{\min(N_t,N_{r,k})} p_{k,l} \\
\text{s.t.} \quad & \sum_{l=1}^{\min(N_t,N_{r,k})} \log_2\left(1+\frac{a_{k,l}}{b_{k,l}+e_{k,l}+\sigma^2}\right) \geq \lambda_k, \forall k, \\
& \sum_{k=1}^{K}\sum_{l=1}^{\min(N_t,N_{r,k})} p_{k,l} \leq P_{\max},
\end{aligned} \tag{P1.2}$$

where $a_{k,l}$, $b_{k,l}$, and $e_{k,l}$ represent the strength, inter-user interference, and intra-user interference expressions, as defined in (P1).

To derive a convex formulation of (P1.2), we perform the following steps:

1) Defining $\min(N_t, N_{r,k})$ number of auxiliary variables, i.e., $\lambda_{k,l}$, for all k, l.

$$\begin{aligned}
\min_{\mathbf{w}_{k,l},\mathbf{f}_{k,l},L_k,p_{k,l}} \quad & \sum_{k=1}^{K}\sum_{l=1}^{L_k} p_{k,l} \\
\text{s.t.} \quad & \sum_{l=1}^{L_k} \log_2\left(1+\frac{|\mathbf{f}_{k,l}\mathbf{H}_k^H \mathbf{w}_{k,l}|^2}{\sum_{j\neq l}^{L_k}|\mathbf{f}_{k,l}\mathbf{H}_k^H \mathbf{w}_{k,j}|^2+\sum_{i\neq k}^{K}\sum_{m=1}^{L_i}|\mathbf{f}_{k,l}\mathbf{H}_k^H \mathbf{w}_{i,m}|^2+\sigma^2}\right) \geq \lambda_k, \quad \forall k, \\
& \sum_{k=1}^{K}\sum_{l=1}^{L_k} \|\mathbf{w}_{k,l}\|^2 \leq P_{\max}.
\end{aligned} \tag{P1.1}$$

$$c_k = \sum_{l=1}^{L_k} \log_2\left(1+\frac{\mathbf{f}_{k,l}^H \mathbf{H}_k^H \mathbf{w}_{k,l}\mathbf{w}_{k,l}^H \mathbf{H}_k \mathbf{f}_{k,l}}{\sum_{\substack{j=1\\ j\neq l}}^{L_k} \mathbf{f}_{k,l}^H \mathbf{H}_k^H \mathbf{w}_{k,j}\mathbf{w}_{k,j}^H \mathbf{H}_k \mathbf{f}_{k,l} + \sum_{\substack{i=1\\ i\neq k}}^{K}\sum_{m=1}^{L_i} \mathbf{f}_{k,l}^H \mathbf{H}_k^H \mathbf{w}_{i,m}\mathbf{w}_{i,m}^H \mathbf{H}_k \mathbf{f}_{k,l}+\sigma^2}\right), \tag{2}$$

2) Replacing λ_k by $\sum_{l=1}^{L_k} \lambda_{k,l}$, for all k.
3) Extracting $\sum_{l=1}^{L_k} \lambda_{k,l} = \lambda_k$, for all k, as a separate constraint.

Thus, the convex formulation of (P1.2) can be easily derived in (P1.3), as shown at the bottom of the next page. Given $\lambda_{k,l}$ and $p_{k,l}$, $\forall k, l$, from (P1.3), the optimal L_k and p_k, $\forall k$, can be calculated as $\left[p_{k,1}, \cdots, p_{k,\min(N_t,N_{r,k})}\right] > 0$ and $\sum_{l=1}^{\min(N_t,N_{r,k})} p_{k,l}, \forall k$, respectively.

A more refined explanation of the optimization process for $w_{k,l}$, $f_{k,l}$, L_k, and $p_{k,l}$ is presented through a four-step AO algorithm, as outlined in Algorithm 1. When provided with the initial values for $w_{k,l}$, F_k, L_k, and p_k obtained from (3), (4), and (P1.3), the problem (P1) can be expressed as (P1.4), as shown at the bottom of the next page. In the following subsection, we tackle (P1.4) by developing a solution for Φ.

B. OPTIMIZATION OF RIS PHASES

To optimize the RIS, we first perform the traditional steps [4], [5], [12], [19], i.e., change of variables and SDR. 1) Following the change of variables

$$\begin{aligned}
f_{k,l}^H H_{r,k}^H \Phi G w_{i,m} &= l^H \omega^{kl,im} f_{k,l}^H H_{d,k}^H w_{i,m} &= \xi^{kl,im},\\
f_{k,l}^H H_{r,k}^H \Phi G w_{k,j} &= l^H \omega^{kl,kj} f_{k,l}^H H_{d,k}^H w_{k,j} &= \xi^{kl,kj},\\
f_{k,l}^H H_{r,k}^H \Phi G w_{k,l} &= l^H \omega^{kl,kl} f_{k,l}^H H_{d,k}^H w_{k,l} &= \xi^{kl,kl},
\end{aligned}$$

where $\omega^{kl,im} = \operatorname{diag}\left(f_{k,l}^H H_{r,k}^H\right) G w_{i,m}$, $\omega^{kl,kj} = \operatorname{diag}\left(f_{k,l}^H H_{r,k}^H\right) G w_{k,j}$, $\omega^{kl,kl} = \operatorname{diag}\left(f_{k,l}^H H_{r,k}^H\right) G w_{k,l}$, and $l^H = \left[e^{-j\phi_1}, e^{-j\phi_2}, \cdots, e^{-j\phi_N}\right]$, (P1.4) for l can be written as (P1.5), as shown at the bottom of the next page.

Defining $\Theta^{kl,kl} = \begin{bmatrix} \omega^{kl,kl}\omega^{kl,klH} & \omega^{kl,kl}\xi^{kl,klH} \\ \omega^{kl,klH}\xi^{kl,kl} & 0 \end{bmatrix}$, $\Theta^{kl,im} = \begin{bmatrix} \omega^{kl,im}\omega^{kl,imH} & \omega^{kl,im}\xi^{kl,imH} \\ \omega^{kl,imH}\xi^{kl,im} & 0 \end{bmatrix}$, $\Theta^{kl,kj} = \begin{bmatrix} \omega^{kl,kj}\omega^{kl,kjH} & \omega^{kl,kj}\xi^{kl,kjH} \\ \omega^{kl,kjH}\xi^{kl,kj} & 0 \end{bmatrix}$, $\bar{\mathbf{l}} = \begin{bmatrix} \mathbf{l} \\ t \end{bmatrix}$, and noting that $\bar{\mathbf{l}}^H \Theta \bar{\mathbf{l}} = \operatorname{Tr}(\Theta \bar{\mathbf{l}}\bar{\mathbf{l}}^H) = \operatorname{Tr}(\Theta \mathbf{L})$. By relaxing the rank-1 constraint, where t is an auxiliary variable, we obtain the semidefinite expressions for the numerator and denominator of (P1.5) as (P1.5a), as shown at the bottom of the 7th page. where the presence of fractions retains a non-convex nature, leading to a non-convex problem. Utilizing fractional programming techniques [37], we derive an equivalent formulation of (P1.5a) as shown in (P1.6), as shown at the bottom of the 7th page. In (P1.6), y_{kl}, $\forall k, l$, represents extra optimization variables that serve as weights requiring optimization for optimal results. Despite its simplified nature, (P1.6) still faces challenges:

1) Log-sum expressions are computationally expensive to solve, detailed further in [38].
2) As part of the multistep AO algorithm, solving (P1.6) does not guarantee convergence, necessitating modification.
3) Inclusion of y_{kl} results in a bilinear non-convex expression, hence requires convex relaxation or an iterative method.

To address the first issue, we replace log-sum expressions with the geometric mean (GM), as demonstrated in [38]. Defining $x_L^k = \left[x_L^{k,1}, \cdots, x_L^{k,L_k}\right]$, where

$$\begin{aligned}
x_L^{k,l} &= 1 + 2y_{kl}\left(\operatorname{trace}\left(\Theta^{kl,kl} L\right) + \left|\xi^{kl,kl}\right|^2\right)\\
&\quad - y_{kl}^2 \sum_{i\neq k}^{K} \sum_{m=1}^{L_i} \left(\operatorname{trace}\left(\Theta^{kl,im} L\right) + \left|\xi^{kl,im}\right|^2\right)\\
&\quad - y_{kl}^2 \sum_{i\neq k}^{K} \left(\operatorname{trace}\left(\Theta^{kl,kj} L\right) + \left|\xi^{kl,kj}\right|^2\right) + \sigma^2, \quad \forall k, l
\end{aligned}$$

The objective function of (P1.6), i.e.,

$$\begin{aligned}
&\sum_{k=1}^{K} \sum_{l=1}^{L_k} \log_2 \Bigg(1 + 2y_{kl}\operatorname{trace}\left(\Theta^{kl,kl} L\right) + \left|\xi^{kl,kl}\right|^2\\
&\quad - y_{kl}^2 \sum_{i\neq k}^{K} \left(\operatorname{trace}\left(\Theta^{kl,kj} L\right) + \left|\xi^{kl,kj}\right|^2\right)\Bigg)\\
&\quad - y_{kl}^2 \sum_{i\neq k}^{K} \sum_{m=1}^{L_i} \left(\operatorname{trace}\left(\Theta^{kl,im} L\right) + \left|\xi^{kl,im}\right|^2\right) + \sigma^2
\end{aligned}$$

can be replaced by

$$\sum_{k=1}^{K} \operatorname{GM}\left(x_L^k\right)$$

and the problem (P1.6) is updated as follows:

$$\begin{aligned}
\max_{L, y_{kl}} \quad & \sum_{k=1}^{K} \operatorname{GM}\left(x_L^k\right)\\
\text{s.t.} \quad & \operatorname{GM}\left(x_L^k\right) \geq \lambda_k, \forall k \quad L \succeq 0,\ y_{kl} \in \mathbb{R},\ \forall k, l,\\
& L_{(n,n)} = 1,\ n = 1, \cdots, N+1. \qquad \text{(P1.7)}
\end{aligned}$$

To address the second issue, concerning convergence behavior, we update (P1.7) as follows:

$$\begin{aligned}
\max_{L, y_{kl}} \quad & \sum_{k=1}^{K} o_L^k\\
\text{s.t.} \quad & \operatorname{GM}\left(x_L^k\right) \geq \zeta^k + o_L^k, \forall k,\\
& L \succeq 0,\ y_{kl} \in \mathbb{R},\ \forall k, l,\\
& L_{(n,n)} = 1,\ n = 1, \cdots, N+1, \qquad \text{(P1.8)}
\end{aligned}$$

where ζ^k, $\forall k$, represents a positive real number selected in each AO algorithm iteration, ensuring the objective value does not increase and thereby guaranteeing convergence, whereas o_L^k denotes a slack variable, introduced for notational simplicity. Additional details on the selection of ζ^k can be found in Algorithm 1.

To address the third issue of bilinear non-convexity, we propose solving (P1.8) using a nested two-step iterative method. The details are provided in Algorithm 1. Due to the GM expressions, (P1.8) necessitates a lower computational cost compared to (P1.6) with log-sum expressions. Further insights into convergence behavior and computational complexity are discussed in Sections VI and VIII.

IV. USER GROUPING METHOD FOR RIS-ASSISTED MULTIUSER MIMO

Traditional AO approaches, as introduced in works like [4], [13], [28], typically involve solving an optimization problem iteratively for all users until either convergence is achieved or the problem becomes unsolvable. However, a key motivation behind incorporating RIS is to assist users that lack strong direct links to the AP. In such cases, the RIS can act as the primary enabler of communication for these users. On the other hand, due to the inherent multiplicative fading nature of RIS-assisted channels [39], some users may experience minimal or no effective gains from the RIS.

This insight leads to a practical strategy for grouping users based on their channel characteristics in RIS-assisted systems. By identifying users who benefit differently from the direct and reflected links, we can simplify the overall optimization task.

Rather than applying AO to all users, we first analyze the channel conditions, divide users into meaningful groups, and then selectively apply optimization to the most

$$
\begin{aligned}
\min_{p_{k,l},\lambda_{k,l}} \quad & \sum_{k=1}^{K} \sum_{l=1}^{\min(N_t,N_{r,k})} p_{k,l} \\
\text{s.t.} \quad & p_{k,l}\left|\mathbf{f}_{k,l}^H \mathbf{H}_k^H \overline{\mathbf{w}}_{k,l}\right|^2 - (2^{\lambda_{k,l}}-1)\Bigg(\sum_{i\neq k}^{K} \sum_{m=1}^{\min(N_t,N_{r,i})} p_{i,m}\left|\mathbf{f}_{k,l}^H \mathbf{H}_k^H \overline{\mathbf{w}}_{i,m}\right|^2 \\
& + \sum_{j\neq l}^{\min(N_t,N_{r,k})} p_{k,j}\left|\mathbf{f}_{k,l}^H \mathbf{H}_k^H \overline{\mathbf{w}}_{k,j}\right|^2 + \sigma^2\Bigg) \geq 0, \quad \forall k, l \\
& \sum_{l=1}^{\min(N_t,N_{r,k})} \lambda_{k,l} = \lambda_k, \quad \forall k, \quad \sum_{k=1}^{K} \sum_{l=1}^{\min(N_t,N_{r,k})} p_{k,l} \leq P_{\max}.
\end{aligned} \tag{P1.3}
$$

$$
\begin{aligned}
\max_{\Phi} \quad & \sum_{k=1}^{K}\sum_{l=1}^{L_k} \log_2\left(1 + \frac{p_{k,l}\left|\mathbf{f}_{k,l}^H \mathbf{H}_k^H \overline{\mathbf{w}}_{k,l}\right|^2}{\sum_{i\neq k}^{K}\sum_{m=1}^{L_i} p_{i,m}\left|\mathbf{f}_{k,l}^H \mathbf{H}_k^H \overline{\mathbf{w}}_{i,m}\right|^2 + \sum_{j\neq l}^{L_k} p_{k,j}\left|\mathbf{f}_{k,l}^H \mathbf{H}_k^H \overline{\mathbf{w}}_{k,j}\right|^2 + \sigma^2}\right) \\
\text{s.t.} \quad & c_k \geq \lambda_k, \quad \forall k, \\
& \mathbf{H}_k^H = \mathbf{H}_{r,k}^H \Phi \mathbf{G} + \mathbf{H}_{d,k}^H, \\
& \Phi = \operatorname{diag}(e^{j\phi_1}, \ldots, e^{j\phi_N}).
\end{aligned} \tag{P1.4}
$$

$$
\begin{aligned}
\max_{\mathbf{l}} \quad & \sum_{k=1}^{K}\sum_{l=1}^{L_k} \log_2\left(1 + \frac{e_k}{r_k + q_k + \sigma^2}\right) \\
\text{s.t.} \quad & c_k \geq \lambda_k, \quad \forall k, \\
& |\mathbf{l}_n| = 1, \quad n = 1, \ldots, N, \\
& e_k = \mathbf{l}^H \omega^{kl,kl} \omega^{kl,kl^H} \mathbf{l} + \mathbf{l}^H \omega^{kl,kl} \xi^{kl,kl^H} + \xi^{kl,kl} \omega^{kl,kl^H} \mathbf{l} + |\xi^{kl,kl}|^2, \\
& r_k = \sum_{i\neq k}^{K}\sum_{m=1}^{L_i} \left(\mathbf{l}^H \omega^{kl,im} \omega^{kl,im^H} \mathbf{l} + \xi^{kl,im} \omega^{kl,im^H} \mathbf{l} + \mathbf{l}^H \omega^{kl,im} \xi^{kl,im^H} + |\xi^{kl,im}|^2\right), \\
& q_k = \sum_{j\neq l}^{L_k} \left(\mathbf{l}^H \omega^{kl,kj} \omega^{kl,kj^H} \mathbf{l} + \mathbf{l}^H \omega^{kl,kj} \xi^{kl,kj^H} + \xi^{kl,kj} \omega^{kl,kj^H} \mathbf{l} + |\xi^{kl,kj}|^2\right).
\end{aligned} \tag{P1.5}
$$

Algorithm 1 Multi-Step AO Algorithm for Solving (P1)

Initialize:

iteration $i = 0$, $\Phi_i = \mathbf{I}_\Phi$, $L_{i,k} = \min(N_t, N_{r,k})$, $o^k_{\mathbf{L},i} = 0$, $\forall k$.

$\mathbf{W}_i = \frac{1}{\sqrt{N_t}} \left[\mathbf{1}, \mathbf{1}, \ldots, \mathbf{1}_{1,L_1}, \ldots, \mathbf{1}_{K,L_K}\right]^T$

$\mathbf{p}_i = \frac{P_{\max}}{\sum_{k=1}^{K} \min(N_t, N_{r,k})} \left[1, 1, \ldots, 1_{1,L_1}, \ldots, 1_{K,L_K}\right]$

repeat
 Step 1: Given Φ_i, compute the composite channel $\mathbf{H}_k$ for all k.
 repeat
  Step 2a: Given $\mathbf{p}_i$, $L_{i,k}$, and $\mathbf{w}_i$, calculate $\mathbf{F}_{k,i}$ for all k using (4).
  Step 2b: Given $\mathbf{F}_{k,i}$ for all k, $L_{i,k}$, and $\mathbf{p}_i$, update $\mathbf{w}_i$ using (3).
  Step 2c: Update $L_{i,k}$ as $[\lambda_{k,1}, \ldots, \lambda_{k,\min(N_t,N_{r,k})}] > 0$ for all k.
  Step 2d: Given $L_{i,k}$ for all k, $\mathbf{F}_{k,i}$ for all k, $\mathbf{w}_i$, and $\mathbf{p}_i$, update $\lambda_{k,l}$ using (P1.3).
  Step 2e: Given $L_{i,k}$ for all k, $\mathbf{F}_{k,i}$ for all k, $\mathbf{w}_i$, and $\lambda_{k,l}$, update $\mathbf{p}_i$ using (P1.3).
 until The objective value of (P1.1) converges, or the maximum number of iterations is reached.
 repeat
  Step 3: Given $\mathbf{F}_{k,i}$ for all k, $L_{i,k}$ for all k, $\mathbf{p}_i$, and $\mathbf{W}_i$, calculate $\mathbf{x}^k_{\mathbf{L}}$, set $\zeta_k = \mathrm{GM}(\mathbf{x}^k_{\mathbf{L}})$, fix Φ_i, solve (P1.8), and obtain y_{kl}.
  Step 4: Given $\mathbf{F}_{k,i}$ for all k, $L_{i,k}$ for all k, $\mathbf{p}_i$, and $\mathbf{W}_i$, calculate $\mathbf{x}^k_{\mathbf{L}}$, set $\zeta_k = \mathrm{GM}(\mathbf{x}^k_{\mathbf{L}})$, fix y_{kl}, solve (P1.8), and extract Φ_{i+1} from $\mathbf{L}$.
 until The objective value of (P1.8) converges, or the maximum number of iterations is reached.
 Step 5: Update iteration $i = i + 1$.
until The objective value of (P1) converges, or the maximum number of iterations is reached.

relevant categories. This approach can significantly reduce computational complexity while maintaining near-optimal system performance, as will be analyzed in the numerical section.

To implement this strategy, we introduce two user grouping techniques: the 3-user grouping (3-UG) and 2-user grouping (2-UG) methods.

A. THREE GROUPS

In this approach, we split the users into three categories: A, B, and C. An illustration of the system model using the 3-UG method is shown in Fig. 2.

Let $\mathfrak{z}_k$ denote the single-user-optimal RIS configuration for user k, obtained in closed form via the ASB-MIMO rule of Section V applied to user k alone, and define the

$$\max_{\mathbf{L}} \quad \sum_{k=1}^{K} \sum_{l=1}^{L_k} \log_2 \left(1 + \frac{\mathrm{Tr}(\Theta^{kl,kl}\mathbf{L}) + |\xi^{kl,kl}|^2}{\sum\limits_{i \neq k}^{K} \sum\limits_{m=1}^{L_i} \mathrm{Tr}(\Theta^{kl,im}\mathbf{L}) + \sum\limits_{j \neq l}^{L_k} \left(\mathrm{Tr}(\Theta^{kl,kj}\mathbf{L}) + |\xi^{kl,kj}|^2\right) + \sum\limits_{i \neq k}^{K} \sum\limits_{m=1}^{L_i} |\xi^{kl,im}|^2 + \sigma^2} \right)$$
$$\text{s.t.} \quad c_k \geq \lambda_k, \forall k, \quad \mathrm{rank}(\mathbf{L}) = 1, \quad \mathbf{L} \succeq 0, \quad \mathbf{L}_{(n,n)} = 1, \quad n = 1, \ldots, N+1. \tag{P1.5a}$$

$$\begin{aligned} \max_{\mathbf{L}, y_{kl}} \quad & \sum_{k=1}^{K} \sum_{l=1}^{L_k} \Bigg[\log_2 \Big(1 + 2y_{kl}\big(\mathrm{Tr}(\Theta^{kl,kl}\mathbf{L}) + |\xi^{kl,kl}|^2\big) \\ & \quad - y_{kl}^2 \Big(\sum_{i \neq k}^{K} \sum_{m=1}^{L_i} (\mathrm{Tr}(\Theta^{kl,im}\mathbf{L}) + |\xi^{kl,im}|^2) \\ & \quad + \sum_{j \neq l}^{L_k} (\mathrm{Tr}(\Theta^{kl,kj}\mathbf{L}) + |\xi^{kl,kj}|^2) + \sigma^2 \Big)\Big) \Bigg] \\ \text{s.t.} \quad & y_{kl} \in \mathbb{R}, \forall k, l, \quad c_k \geq \lambda_k, \forall k, \quad \mathbf{L} \succeq 0, \quad \mathbf{L}_{(n,n)} = 1, \quad n = 1, \ldots, N+1. \end{aligned} \tag{P1.6}$$

Algorithm 2 3-UG-Based AO Algorithm for Solving (P1)

Initialize:

iteration $i = 0$, $\Phi_i = \mathbf{I}_\Phi$, $L_{i,k} = \min(N_t, N_{r,k})$, $o^k_{\mathbf{L},i} = 0$, $\forall k$.

$\mathbf{W}_i = \frac{1}{\sqrt{N_t}} \left[\mathbf{1}, \mathbf{1}, \ldots, \mathbf{1}_{1,L_1}, \ldots, \mathbf{1}_{K,L_K}\right]^T$

$\mathbf{p}_i = \frac{P_{\max}}{\sum_{k=1}^{K} \min(N_t, N_{r,k})} \left[1, 1, \ldots, 1_{1,L_1}, \ldots, 1_{K,L_K}\right]$

For each user k, compute the single-user-optimal RIS configuration 2_k in closed form via the ASB-MIMO rule (Section V), then form the reflected-to-direct ratio $\gamma_k = \|\mathbf{H}^H_{r,k} 2_k \mathbf{G}\|^2 / \|\mathbf{H}^H_{d,k}\|^2$ defined in (10), and assign k to:

- category **A** if $\gamma_k \le \tau$ (direct link dominates),
- category **C** if $\tau < \gamma_k \le \kappa\tau$ (intermediate),
- category **B** if $\gamma_k > \kappa\tau$ (reflected link dominates),

where $\kappa > 1$ quantifies the "$\gg$" relation (set to $\kappa = 10$ in the simulations).

repeat
    Step 1: Given Φ_i, compute the composite channel $\mathbf{H}_k$ for all k.
    repeat
        Step 2a: Given $\mathbf{p}_i$, $L_{i,k}$, and $\mathbf{w}_i$, calculate $\mathbf{F}_{k,i}$ for all k using (4).
        Step 2b: Given $\mathbf{F}_{k,i}$ for all k, $L_{i,k}$, and $\mathbf{p}_i$, update $\mathbf{w}_i$ using (3).
        Step 2c: Update $L_{i,k}$ as $[\lambda_{k,1}, \ldots, \lambda_{k,\min(N_t,N_{r,k})}] > 0$ for all k.
        Step 2d: Given $L_{i,k}$ for all k, $\mathbf{F}_{k,i}$ for all k, $\mathbf{w}_i$, and $\mathbf{p}_i$, update $\lambda_{k,l}$ using (P1.3).
        Step 2e: Given $L_{i,k}$ for all k, $\mathbf{F}_{k,i}$ for all k, $\mathbf{w}_i$, and $\lambda_{k,l}$, update $\mathbf{p}_i$ using (P1.3).
    until The objective value of (P1.1) converges, or the maximum number of iterations is reached.
    repeat
        Perform Steps 3 and 4 of Algorithm 1 for $k \in \{B, C\}$ only.
    until The objective value of (P1.8) converges or the maximum number of inner iterations is reached.
    Step 5: Update the iteration counter: $i \leftarrow i + 1$.
until The objective value of (P1) converges or the maximum number of outer iterations is reached.

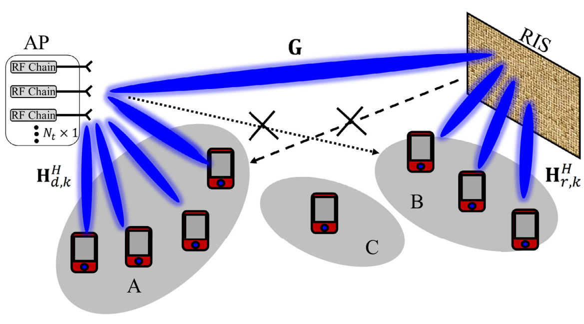

FIGURE 2. Three-category user grouping strategy (3-UG).

reflected-to-direct ratio

$$\gamma_k \triangleq \frac{\left\| H^H_{r,k} 2_k G \right\|^2}{\left\| H^H_{d,k} \right\|^2}. \tag{10}$$

Using a base threshold $\tau > 0$ and a separation factor $\kappa > 1$, the users are partitioned into the following three categories:

- **Group A (direct link dominates):** $\gamma_k \le \tau$.
- **Group C (intermediate):** $\tau < \gamma_k \le \kappa\tau$.
- **Group B (reflected link dominates):** $\gamma_k > \kappa\tau$.

Here, τ governs the boundary between Group A and the remaining users (i.e., whether RIS optimization is beneficial for user k at all), while κ governs the boundary between Group B and Group C. Group B uses the approximation $\mathbf{H}^H_k \approx \mathbf{H}^H_{r,k} 2\mathbf{G}$ in which the direct channel is dropped, and this approximation is accurate only when the reflected channel dominates the direct one by a factor of at least κ. Users with $\tau < \gamma_k \le \kappa\tau$ (Group C) are still included in (P1.8) but with the full composite channel $\mathbf{H}^H_k \approx \mathbf{H}^H_{r,k} 2\mathbf{G} + \mathbf{H}^H_{d,k}$. The 2-UG variant of Section IV-B corresponds to the special case $\kappa = 1$ in which Group C is empty.

This classification helps reduce the computational effort in each AO iteration as follows:

1) Rather than recalculating the full composite channel for every user, we approximate it differently for each group:
   - For Group A: $H^H_k \approx H^H_{d,k}$,
   - For Group B: $H^H_k \approx H^H_{r,k} \Theta G$,
   - For Group C: $H^H_k \approx H^H_{r,k} \Theta G + H^H_{d,k}$.
2) We solve problem (P1.8) only for users in Groups B and C, which proportionally reduces the number of constraints in the problem. More specifically, with the 3-UG method, problem (P1.8) can be simplified as follows:

$$\begin{aligned} &\max_{L,\, y_{kl}} \sum_{k \in \{\mathrm{B},\, \mathrm{C}\}} o^k_L \\ &\text{s.t.} \quad \mathrm{GM}\left(x^k_L\right) \ge \zeta^k + o^k_L, \quad \forall k \in \{\mathrm{B},\, \mathrm{C}\}, \\ &\qquad L \succeq 0, \quad y_{kl} \in \mathbb{R}, \quad \forall k, l \in \{\mathrm{B},\, \mathrm{C}\}, \\ &\qquad L_{(n,n)} = 1, \quad \forall n = 1, \ldots, N+1, \end{aligned} \tag{P1.9}$$

Algorithm 3 2-UG-Based AO Algorithm for Solving (P1)

Initialize:

iteration $i = 0$, $\Phi_i = \mathbf{I}_\Phi$, $L_{i,k} = \min(N_t, N_{r,k})$, $o^k_{\mathbf{L},i} = 0$, $\forall k$.

$\mathbf{W}_i = \frac{1}{\sqrt{N_t}}\left[\mathbf{1}, \mathbf{1}, \ldots, \mathbf{1}_{1,L_1}, \ldots, \mathbf{1}_{K,L_K}\right]^T$

$\mathbf{p}_i = \frac{P_{\max}}{\sum_{k=1}^{K}\min(N_t, N_{r,k})}\left[1, 1, \ldots, 1_{1,L_1}, \ldots, 1_{K,L_K}\right]$

For each user k, compute the single-user-optimal RIS configuration $\mathfrak{z}_k$ in closed form via the ASB-MIMO rule (Section V), then form the reflected-to-direct ratio γ_k as in (10). Assign k to category **B** if $\gamma_k > \tau$ (reflected link dominates); otherwise, i.e., if $\gamma_k \leq \tau$, assign k to category **A** (direct link dominates).

repeat
  Step 1: Given Φ_i, compute the composite channel $\mathbf{H}_k$ for all k.
  repeat
    Step 2a: Given $\mathbf{p}_i$, $L_{i,k}$, and $\mathbf{w}_i$, calculate $\mathbf{F}_{k,i}$ for all $k \in \{A, B\}$ using (4).
    Step 2b: Given $\mathbf{F}_{k,i}$ for all $k \in \{A, B\}$, $L_{i,k}$, and $\mathbf{p}_i$, update $\mathbf{w}_i$ using (3).
    Step 2c: Update $L_{i,k}$ as $[\lambda_{k,1}, \ldots, \lambda_{k,\min(N_t,N_{r,k})}] > 0$ for all $k \in \{A, B\}$.
    Step 2d: Given $L_{i,k}$ for all k, $\mathbf{F}_{k,i}$ for all $k \in \{A, B\}$, $\mathbf{w}_i$, and $\mathbf{p}_i$, update $\lambda_{k,l}$ using (P1.3).
    Step 2e: Given $L_{i,k}$ for all $k \in \{A, B\}$, $\mathbf{F}_{k,i}$ for all k, $\mathbf{w}_i$, and $\lambda_{k,l}$, update $\mathbf{p}_i$ using (P1.3).
  until The objective value of (P1.1) converges, or the maximum number of iterations is reached.
  repeat
    Perform Steps 3 and 4 of Algorithm 1 for $k \in \{B\}$ only.
  until The objective value of (P1.8) converges or the maximum number of inner iterations is reached.
  Step 5: Update the iteration counter: $i \leftarrow i + 1$.
until The objective value of (P1) converges or the maximum number of outer iterations is reached.

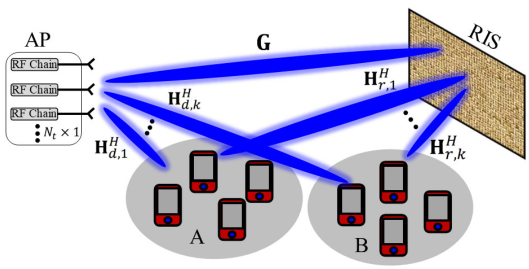

FIGURE 3. Two-category user grouping strategy (2-UG).

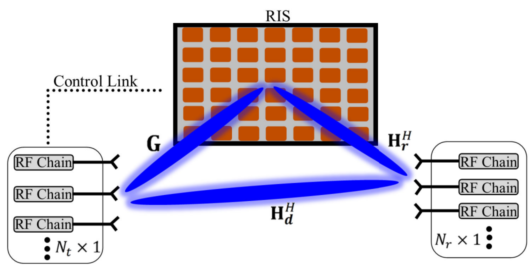

FIGURE 4. RIS-assisted P2P MIMO.

B. TWO GROUPS

The 2-UG approach divides the users into two categories based on the relative strength of their reflected and direct channels. The corresponding system model is shown in Fig. 3.

For classification, we again use the reflected-to-direct ratio γ_k defined in (10), which is evaluated with the closed-form single-user-optimal RIS configuration $\mathfrak{z}_k$ (see Section IV-A and Section V), and apply a single threshold $\tau > 0$. If $\gamma_k > \tau$, user k is assigned to Group B (reflected link dominates); otherwise, i.e., if $\gamma_k \leq \tau$, user k is assigned to Group A (direct link dominates). These two conditions are mutually exclusive and exhaustive. Specifically, in each iteration, we solve problem (P1.8) only for users in Group B, which simplifies (P1.8) as follows:

$$\begin{aligned}
&\max_{L,\, y_{kl}} \sum_{k\in\{\mathrm{B}\}} o^k_L \\
&\text{s.t.} \quad \mathrm{GM}\left(x^k_L\right) \geq \zeta^k + o^k_L, \quad \forall k \in \{\mathrm{B}\}, \\
&\qquad L \succeq 0, \quad y_{kl} \in \mathbb{R}, \quad \forall k, l \in \{\mathrm{B}\}, \\
&\qquad L_{(n,n)} = 1, \quad \forall n = 1, \ldots, N+1, \qquad \text{(P1.10)}
\end{aligned}$$

V. ADAPTIVE SELECTION FOR RIS-ASSISTED P2P MIMO

In this section, we extend the UG concept to a P2P MIMO scenario and develop a low-complexity beamforming solution. Building on this, we propose a non-iterative algorithm that achieves near-optimal performance with significantly reduced computational complexity.

Before introducing the proposed approach, we briefly review the RIS-assisted P2P MIMO configuration and summarize the existing beamforming technique with the lowest known complexity.

A. SYSTEM MODEL

By setting $K = 1$ in Fig. 1, the system reduces to a single-user scenario, representing a P2P MIMO communication setup. The corresponding system model is illustrated in Fig. 4.

The received signal at the receiver is expressed as:

$$y = W^\dagger \left(H^H_r \Theta G + H^H_d\right) Fs + W^\dagger z, \qquad (11)$$

where $F \in \mathbb{C}^{N_t \times N_s}$ is the transmit beamforming matrix, $W \in \mathbb{C}^{N_r \times N_s}$ is the receive beamforming matrix, N_s denotes the number of data streams, and z is the additive noise vector. The corresponding channel capacity is given by:

$$c = \log_2 \det\left(I_{N_s} + W^{\dagger} H F F^H H^H W\right), \tag{12}$$

where the composite channel matrix is defined as:

$$H = H_r^H \Theta G + H_d^H. \tag{13}$$

B. PROBLEM FORMULATION AND EXISTING SOLUTIONS

To maximize the c in (12), we need to optimize the beamforming matrices F, W, and the phase matrix Θ. Therefore, the problem can be formulated as follows:

$$\begin{aligned} \max_{F,W,\Theta} \; & \log_2 \det\left(I_{N_s} + \frac{1}{\sigma^2} W^{\dagger} H F F^H H^H W\right) \\ \text{s.t.} \quad & H = H_r^H \Theta G + H_d^H, \\ & \Theta = \operatorname{diag}\left(e^{-j\phi_1}, e^{-j\phi_2}, \ldots, e^{-j\phi_N}\right), \\ & \|F\|^2 \le P_{\max}, \end{aligned} \tag{P2}$$

where $P_{\max}$ represents the maximum transmit power.

The problem (P2) has been extensively studied in the literature [4], [29]. Standard methods such as SDR, manifold optimization, and gradient descent combined with water-filling and singular value decomposition (SVD) can be used to derive optimal solutions for (P2). However, the algorithms based on these methods tend to be iterative and computationally complex.

The least complex solution in the literature is based on closed-form solutions [4], [29]. Specifically, under assumptions such as a low SNR regime and/or small-scale MIMO, it is optimal to allocate all available transmit power to the strongest data stream in the P2P MIMO setup, focusing solely on the diversity gains. With these assumptions, (P2) allows for a closed-form solution for Θ, where the receive combiner w_{n_s} and the transmit precoder f_{n_s} are selected as the left and right dominant singular vectors of H, respectively. Despite the closed-form solutions, the algorithm remains iterative. The iterative nature of the algorithms in the context of RIS problems is difficult to avoid, as the variables depend on each other, requiring alternating optimization techniques.

In the following section, we discuss how the proposed UG concept can help alleviate this dependency and propose a non-iterative, low-complexity algorithm. However, before that, we briefly discuss the existing low-complexity solution to (P2), which also serves as a benchmark.

C. AO-MIMO: EXISTING LOW-COMPLEXITY SOLUTION TO (P2)

As discussed, the lowest complexity solution is optimal for low SNR and/or small-scale MIMO scenarios. For these cases, it is optimal to consider a single data stream and allocate all power to it. Corresponding to this simplicity, the problem (P2) can be simplified as follows:

$$\begin{aligned} \max_{\Theta} \; & \log_2\left(1 + \frac{1}{\sigma^2}\left|w_{n_s}^* \left(H_r^H \Theta G + H_d^H\right) f_{n_s}\right|^2\right) \\ \text{s.t.} \quad & \Theta = \operatorname{diag}\left(e^{-j\phi_1}, e^{-j\phi_2}, \ldots, e^{-j\phi_N}\right), \\ & \left\|f_{n_s}\right\|^2 = P_t, \end{aligned} \tag{P2.1}$$

where $w_{n_s} \in \mathbb{C}^{N_r \times 1}$ and $f_{n_s} \in \mathbb{C}^{N_t \times 1}$ denote, respectively, the dominant *left* and *right* singular vectors of H (i.e., the receive combiner and the transmit precoder corresponding to the strongest spatial mode), and n_s is the index of the strongest data stream, i.e., corresponding to the largest singular value. Following the change of variables:

$$w_{n_s}^* H_d^H f_{n_s} = \eta_{n_s},$$
$$w_{n_s}^* H_r^H \Theta G f_{n_s} = l^H \alpha_{n_s},$$

where

$$l^H = \left[e^{-j\phi_1}, e^{-j\phi_2}, \ldots, e^{-j\phi_N}\right],$$

and

$$\alpha_{n_s} = \operatorname{diag}\left(w_{n_s}^* H_r^H\right) G f_{n_s},$$

we can rewrite the problem (P2.1) as:

$$\begin{aligned} \max_{l} \; & \log_2\left(1 + \frac{1}{\sigma^2}\left|l^H \alpha_{n_s} + \eta_{n_s}\right|^2\right) \\ \text{s.t.} \; & |l_n| = 1, \quad n = 1, \ldots, N, \end{aligned} \tag{P2.2}$$

which is equivalent to:

$$\begin{aligned} \max_{l} \; & \left|l^H \alpha_{n_s} + \eta_{n_s}\right|^2 \\ \text{s.t.} \; & |l_n| = 1, \quad n = 1, \ldots, N. \end{aligned} \tag{P2.3}$$

It is easy to demonstrate that (P2.3) achieves the upper bound only when:

$$\arg\left(l^H \alpha_{n_s}\right) = \arg\left(\eta_{n_s}\right). \tag{14}$$

Hence, the optimal solution to (P2.3) is given by:

$$l^H = e^{j\left(\arg(\eta_{n_s}) - \arg(\alpha_{n_s})\right)},$$

or element-wise:

$$\begin{aligned} \phi_n^* &= \arg\left(\eta_{n_s}\right) - \arg\left(\alpha_{n_s}(n)\right), \quad n = 1, \ldots, N, \\ &= \arg\left(\mathbf{w}_{n_s,a}^* \mathbf{H}_d^H \mathbf{f}_{n_s,a}\right) - \arg\left(\left[\mathbf{w}_{n_s,a}^* \mathbf{H}_r^H\right]_{(n)}\right) \\ &\quad - \arg\left(\mathbf{g}_{(n)}^H \mathbf{f}_{n_s,a}\right), \quad n = 1, \ldots, N. \end{aligned} \tag{15}$$

The AO algorithm based on these results optimizes w, f, and Θ until convergence is achieved. More details on this algorithm can be found in [4], [29].

D. ASB-MIMO: A LOW-COMPLEXITY SOLUTION TO (P2)

We observe that when the impact of the active AP on the user is relatively stronger, the performance received by the user mainly comes from the AP, and the optimization of the RIS has a negligible impact through the backscatter channel $\mathbf{G}2\mathbf{H}_r$. Similarly, when the user is in the strong vicinity of the RIS, the optimization of the transmit and receive digital filters has a negligible impact from the direct channel, i.e., $\mathbf{H}_d$. Based on this observation, we propose to calculate two suboptimal, low-complexity solution candidates for $\mathbf{w}$, $\mathbf{f}$, and 2. These two candidate solutions become optimal depending on the user's relative proximity to the RIS and AP. More specifically, an optimal selection between these two solution sets results in near-optimal performance.

Below, we derive these two solution candidates:

1) FIRST CANDIDATE SOLUTION SET

The first candidate solution set, denoted as set (a) for $\mathbf{w}$, $\mathbf{f}$, and 2 (i.e., $\mathbf{w}_a$, $\mathbf{f}_a$, and 2_a), is selected by considering the dominance of $\mathbf{H}_d$ over $\mathbf{G}2\mathbf{H}_r$. Specifically, we select

$$\mathbf{f}_{n_s,a} = \mathbf{V}_{a(1,:)}\sqrt{P_t}$$

and

$$\mathbf{w}_{n_s,a} = \mathbf{U}_{a(1,:)}$$

where

$$\mathbf{U}_a \Sigma \mathbf{V}_a^H = \text{svd}\left(\mathbf{H}_d^H\right).$$

Inserting $\mathbf{f}_{n_s,a}$ and $\mathbf{w}_{n_s,a}$ into (15), we obtain a low-complexity solution for 2 as follows:

$$\phi^*_{(n),a} = \underbrace{\arg\left(\mathbf{w}^*_{n_s,a}\mathbf{H}_d^H\mathbf{f}_{n_s,a}\right)}_{0} - \arg\left(\left[\mathbf{w}^*_{n_s,a}\mathbf{H}_r^H\right]_{(n)}\right) - \arg\left(\mathbf{g}_{(n)}^H\mathbf{f}_{n_s,a}\right), \quad n = 1, \cdots, N. \tag{16}$$

It reduces to

$$\phi^*_{(n),a} = -\arg\left(\left[\mathbf{w}^*_{n_s,a}\mathbf{H}_r^H\right]_{(n)}\right) - \arg\left(\mathbf{g}_{(n)}^H\mathbf{f}_{n_s,a}\right), \quad n = 1, \cdots, N, \tag{17}$$

which is of lower complexity than (15).

Note that while solution set (a) is derived assuming the dominance of $\mathbf{H}_d$, the impact of the reflecting channel components $\mathbf{H}_r$ and $\mathbf{G}$ is still considered in the optimization of the RIS phases.

2) SECOND CANDIDATE SOLUTION SET

Now we derive the second candidate solution set, denoted as $\mathbf{w}_b$, $\mathbf{f}_b$, and 2_b. This candidate is derived by considering the dominance of the reflecting channel $\mathbf{G}2\mathbf{H}_r$ over the direct channel $\mathbf{H}_d$. Specifically, we select $\mathbf{w}$ and $\mathbf{f}$ as follows:

$$\mathbf{f}_{n_s,b} = \mathbf{V}_{b(1,:)}\sqrt{P_t}$$
$$\mathbf{w}_{n_s,b} = \mathbf{U}_{b(1,:)}$$

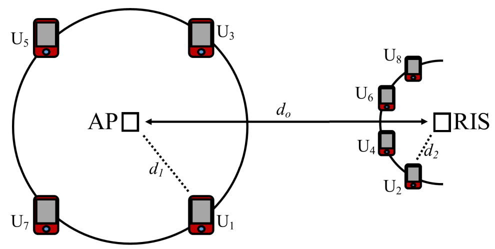

FIGURE 5. Simulation setup for multiuser MIMO.

where

$$\mathbf{U}_b \Sigma \mathbf{V}_b^H = \text{svd}\left(\mathbf{G}\right).$$

Inserting these into (15), we get a low-complexity expression for 2 as follows:

$$\phi^*_{(n),b} = \arg\left(\mathbf{w}^*_{n_s,b}\mathbf{H}_d^H\mathbf{f}_{n_s,b}\right) - \arg\left(\left[\mathbf{w}^*_{n_s,b}\mathbf{H}_r^H\right]_{(n)}\right) - \underbrace{\arg\left(\mathbf{g}_{(n)}^H\mathbf{f}_{n_s,b}\right)}_{0}, \quad n = 1, \cdots, N. \tag{18}$$

which reduces to

$$\phi^*_{(n),b} = \arg\left(\mathbf{w}^*_{n_s,b}\mathbf{H}_d^H\mathbf{f}_{n_s,b}\right) - \arg\left(\left[\mathbf{w}^*_{n_s,b}\mathbf{H}_r^H\right]_{(n)}\right), \quad n = 1, \cdots, N. \tag{19}$$

Note that the candidate solution set (b) is optimized for the dominance of the reflecting channel components $\mathbf{G}$, yet the impact of $\mathbf{H}_r$ and $\mathbf{H}_d$ is still taken into account in the optimization of the RIS phases.

3) SELECTION OF SOLUTION SET BASED ON PERFORMANCE

Now, the third step is to select one of these solution sets based on their performance. More specifically, we select $(\mathbf{w}_a, \mathbf{f}_a, 2_a)$ if

$$\left|\mathbf{l}_a^H \alpha_{n_s,a} + \eta_{n_s,a}\right|^2 > \left|\mathbf{l}_b^H \alpha_{n_s,b} + \eta_{n_s,b}\right|^2,$$

otherwise, we select $(\mathbf{w}_b, \mathbf{f}_b, 2_b)$, where

$$\eta_{n_s,a} = \mathbf{w}^*_{n_s,a}\mathbf{H}_d^H\mathbf{f}_{n_s,a},$$
$$\mathbf{l}_a^H \alpha_{n_s,a} = \mathbf{w}^*_{n_s,a}\mathbf{H}_r^H 2\mathbf{G}\mathbf{f}_{n_s,a},$$
$$\eta_{n_s,b} = \mathbf{w}^*_{n_s,b}\mathbf{H}_d^H\mathbf{f}_{n_s,b},$$
$$\mathbf{l}_b^H \alpha_{n_s,b} = \mathbf{w}^*_{n_s,b}\mathbf{H}_r^H 2\mathbf{G}\mathbf{f}_{n_s,b}.$$

VI. NUMERICAL ANALYSIS-MULTIUSER

A. SIMULATION SETUP

Fig. 5 illustrates the typical simulation setup adopted for RIS-assisted multiuser communication scenarios, where a total of eight users, labeled as U_k for $k = 1, 2, \ldots, 8$, are considered. By default, each user is assigned a spectral efficiency of $\lambda_k = 2$ bps/Hz, and the Rician factor for the AP-to-RIS channel is set to $\chi = -20$ dB. The noise

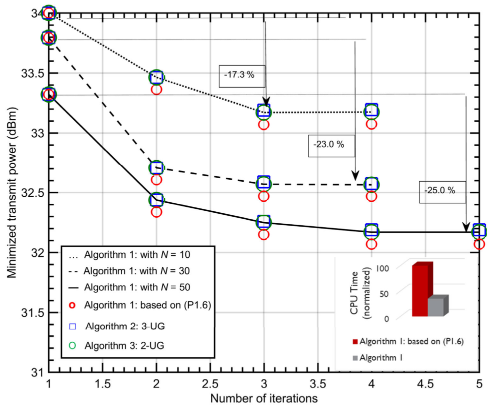

FIGURE 6. **Convergence gap: Minimized transmit power versus the number of iterations for different values of N.**

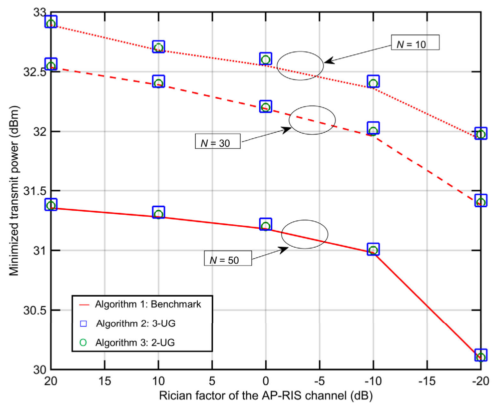

FIGURE 7. **Performance gap: Minimized transmit power versus Rician factor of AP-RIS channel for different values of N.**

power is assumed to be $\sigma_k^2 = -94$ dBm for all users. Each user is equipped with $N_{r,k} = 4$ receive antennas, while the transmitter employs $N_t = 16$ antennas. The reference distances in the setup are $d_o = 40$ m, $d_1 = 20$ m, and $d_2 = 3$ m, with a decision threshold of $\tau = 0.02$ and a separation factor of $\kappa = 10$ for the 3-UG rule of Algorithm 2. Further details on simulation parameters and channel modeling are available in [5]. All performance results are averaged over 50 independent channel realizations and are obtained using MATLAB R2022a on a system powered by an AMD Ryzen R7-5800H processor (3.20 GHz) and 16 GB of RAM.

B. CONVERGENCE AND GEOMETRIC MEAN VERSUS LOG-SUM EXPRESSIONS

Before analyzing the performance and complexity gaps of Algorithms 2 and 3 with respect to Algorithm 1, we first discuss their convergence behavior and highlight the advantage of the derived GM-based convex approximation of the log-sum expression. Specifically, Fig. 6 illustrates the minimized transmit power versus the number of iterations for Algorithms 1, 2, and 3. Additionally, as a benchmark, we also include in Fig. 6 the convergence of Algorithm 1 based on the original log-sum formulation (P1.6).

From Fig. 6, the following observations can be made:

1) Algorithm 1, whether using the geometric mean or the log-sum formulation, converges in a similar number of iterations for a given value of N, with a negligible performance gap.
2) The version of Algorithm 1 based on the geometric mean approximation (P1.8) is up to 70% less computationally complex than the log-sum-based formulation (P1.6).
3) Algorithms 2 and 3, which utilize the proposed UG-based methods, demonstrate similar convergence behavior to Algorithm 1. However, Algorithm 2 (based on the 3-UG method) exhibits a slightly lower performance compared to Algorithms 1 and 3. This minor gap is attributed to the approximation made in Algorithm 2, where the effective channels for users in Groups A and B are computed while neglecting the reflecting and direct components, respectively. Despite this approximation, as seen in Fig. 6, the resulting performance loss is negligible and offers significant gains in computational efficiency.

C. COMPLEXITY

In Table 1, we present a detailed computational complexity analysis of Algorithms 1, 2, and 3 for various values of N and N_t. It can be observed that under the considered simulation setup, i.e., Fig. 5, the proposed UG-based methods, Algorithms 2 and 3, achieve up to 77% reduction in computational complexity compared to Algorithm 1. For example, when $N = 50$ and $N_t = 64$, Algorithms 2 and 3 achieve 75.12% and 73.12% complexity reductions, respectively, relative to Algorithm 1. It is noteworthy that for this specific user distribution scenario, illustrated in Fig. 5, only a subset of users is assigned to Group B, which contributes significantly to the observed complexity reduction. Therefore, in scenarios where the geographic distribution of users lies within close proximity to the AP, the proposed UG-based algorithms can potentially offer near-total complexity reduction without compromising performance.

D. PERFORMANCE

Next, we analyze the performance behavior of Algorithms 2 and 3 for various values of N and different channel conditions. Specifically, in Fig. 7, we plot the minimized transmit power versus the Rician factor of the AP-RIS channel for different values of N. It can be observed that Algorithms 2 and 3, based on the proposed UG methods, maintain performance comparable to the benchmark Algorithm 1 (without the UG method). More specifically, in Fig. 7, we note that Algorithm 2, i.e., the 3-UG method, which categorizes users into three groups, exhibits a slight performance gap, although negligible, compared to Algorithm 3, i.e., the 2-UG method. For instance, at a Rician factor of -20 dB and $N = 50$, Algorithm 1 requires a transmit

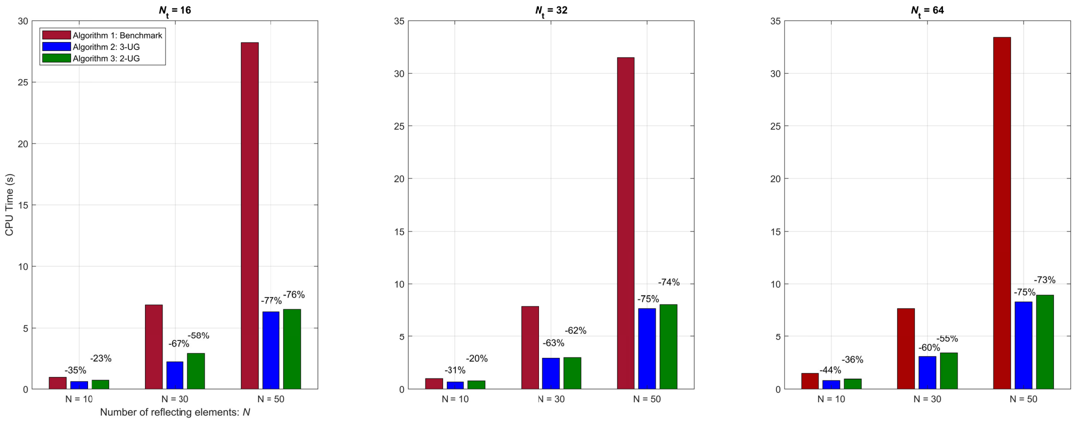

FIGURE 8. Average CPU running time for Algorithms 1, 2, and 3.

TABLE 1. Average CPU running time for Algorithms 1, 2, and 3.

Algorithm	$N_t = 16$			$N_t = 32$			$N_t = 64$		
	$N = 10$	$N = 30$	$N = 50$	$N = 10$	$N = 30$	$N = 50$	$N = 10$	$N = 30$	$N = 50$
Algorithm 1: Benchmark	0.945 s	6.88 s	28.21 s	0.98 s	7.88 s	31.50 s	1.47 s	7.68 s	33.41 s
Algorithm 2: 3-UG	0.61 s	2.20 s	6.32 s	0.67 s	2.91 s	7.68 s	0.81 s	3.07 s	8.31 s
Complexity Reduction	**35.55%**	**67.90%**	**77.60%**	**31.63%**	**63.04%**	**75.56%**	**44.64%**	**60.05%**	**75.12%**
Algorithm 3: 2-UG	0.72 s	2.88 s	6.52 s	0.78 s	2.97 s	8.06 s	0.94 s	3.41 s	8.94 s
Complexity Reduction	**23.10%**	**58.10%**	**76.90%**	**20.41%**	**62.39%**	**74.44%**	**36.08%**	**55.57%**	**73.26%**

power of 30.98 dBm at the AP, while Algorithms 2 and 3 require 31.01 dBm and 31.00 dBm, respectively, demonstrating minimal performance degradation. This negligible performance gap is traded for reduced computational complexity. For example, in Fig. 8, when $N = 50$ and $N_t = 64$, Algorithm 3 achieves a 73.12% complexity reduction, while Algorithm 2 achieves a 75.12% reduction relative to Algorithm 1.

Next, we consider various random locations of UEs in the communication region and plot the CDF of the minimized transmit power required to achieve the target performance rate for different values of N in Fig. 9. In Fig. 9, we observe that both Algorithms 2 and 3 maintain near-optimal performance, i.e., comparable to Algorithm 1, for all random UE locations. Hence, the results in Fig. 9 for a wide range of random geographical locations provide sufficient numerical evidence of the near-optimality of Algorithms 2 and 3 relative to Algorithm 1.

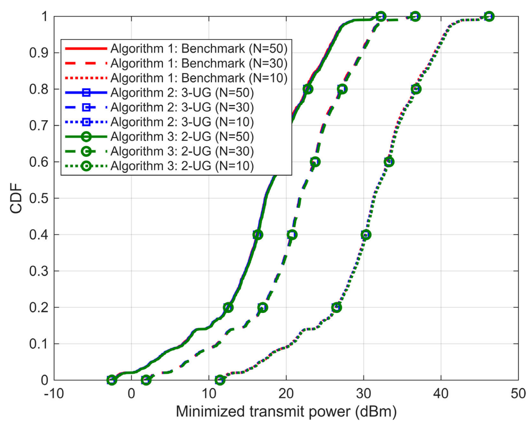

FIGURE 9. CDF of minimized transmit power for various UE geographical locations and different values of N.

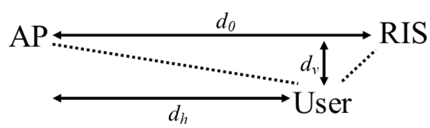

FIGURE 10. Simulation setup for P2P MIMO.

VII. NUMERICAL ANALYSIS-P2P MIMO

A. SIMULATION SETUP

Similar to the setup shown in Fig. 5, we consider a commonly used simulation configuration for P2P MIMO, as illustrated in Fig. 10. The distance between the AP and RIS, denoted by d_o, is fixed at 40 meters. The vertical distance d_v between the user and the line connecting the AP and RIS is set to 2 meters. To examine performance variations, the horizontal distance d_h is varied. Unless otherwise specified, all simulation parameters are identical to those discussed in Section VI.

B. PERFORMANCE AND COMPLEXITY

In Fig. 12, with $N = 50$ and $N_t = N_r = 4$, we plot the achievable rate of the MIMO system while varying d_h, representing different unique geographic locations. The schemes compared in Fig. 12 are described below:

1) AO-MIMO: As discussed in Section V, AO-MIMO is an existing low-complexity solution for RIS-assisted P2P MIMO systems [4], [29], based on

TABLE 2. Average CPU running time for AO-MIMO and ASB-MIMO.

Algorithm	4×4 MIMO			16×16 MIMO			64×64 MIMO		
	$N = 10$	$N = 30$	$N = 50$	$N = 10$	$N = 30$	$N = 50$	$N = 10$	$N = 30$	$N = 50$
AO-MIMO	2.00 ms	2.30 ms	3.90 ms	2.60 ms	2.81 ms	4.34 ms	3.80 ms	4.60 ms	6.30 ms
ASB-MIMO	0.30 ms	0.50 ms	0.70 ms	0.50 ms	0.80 ms	1.10 ms	0.90 ms	1.40 ms	2.10 ms
Complexity Reduction	85%	78%	82%	83%	71%	75%	76%	70%	67%

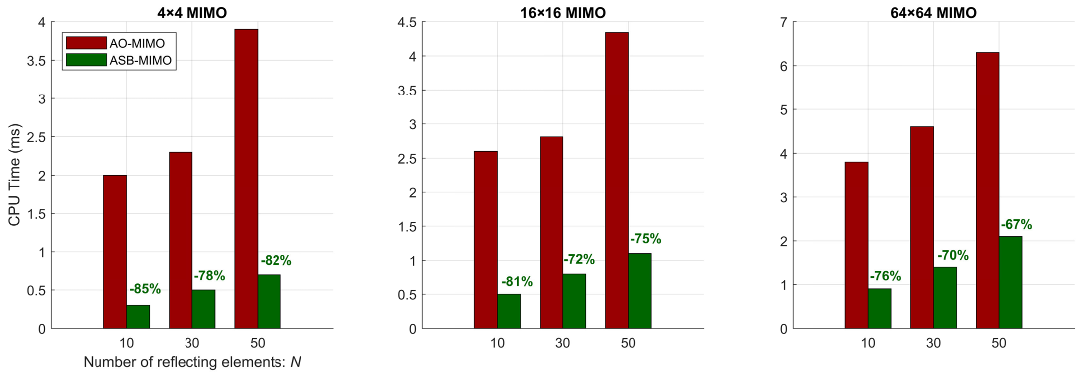

FIGURE 11. Average CPU running time for AO-MIMO and ASB-MIMO.

closed-form expressions. It serves as a benchmark due to its low computational burden and involvement of optimal formulations. Additionally, AO-MIMO provides an upper bound on performance.

2) SDR-MIMO: This scheme utilizes the SDR approach [28]. As observed in Fig. 12, SDR-MIMO shows a minor performance gap compared to AO-MIMO and ASB-MIMO. This gap arises due to rank loss when retrieving a strong rank-1 solution from the relaxed SDP matrix. Moreover, SDR methods are highly computationally expensive, so their complexity analysis is omitted here.
3) ASB-MIMO: The proposed ASB-MIMO scheme demonstrates comparable performance to AO-MIMO across all geographic locations. However, as seen in Table 2, ASB-MIMO achieves a substantial reduction in complexity, up to 85% lower than AO-MIMO. For example, with $N = 50$ and a 4×4 MIMO system, ASB-MIMO offers approximately 82% complexity reduction. This is due to: (1) the derived low-complexity solutions in (P1.5) and (P1.6), and (P1.1) the elimination of iterative calculations.
4) $(\mathbf{w}_a, \mathbf{f}_a, \mathcal{Z}_a)$: In this scheme, the derived candidate solution "a" is fixed across all geographic locations. As shown in Fig. 12, this configuration achieves near-optimal performance only when the receiver is in close proximity to the AP.
5) $(\mathbf{w}_b, \mathbf{f}_b, \mathcal{Z}_b)$: Similarly, this scheme fixes the derived candidate solution "b" for all locations. It performs optimally only when the receiver is near the RIS, and becomes suboptimal otherwise.

In Table 2 and Fig. 11, we present the computational complexity of AO-MIMO and ASB-MIMO for various $N_t \times N_r$ configurations and different values of N, along with the corresponding achieved complexity reductions. As observed in Fig. 11, the proposed ASB-MIMO method offers a remarkable reduction in complexity compared to AO-MIMO. However, the complexity gap narrows as the MIMO size, i.e., $N_t \times N_r$, increases.

For instance, in Fig. 11, when using a 4×4 MIMO system and $N = 50$, the complexity reduction is approximately 82%. This reduction drops to 67% when the MIMO size increases to 64×64. This diminishing gap is attributed to the growing dominance of the computational cost of singular value decomposition (SVD) in large MIMO systems, which overshadows the cost associated with the derivation of the phase shift matrix Φ, thereby reducing the relative benefit of ASB-MIMO over AO-MIMO.

Nevertheless, for practical MIMO sizes such as 4×4, 16×16, and 64×64, the proposed ASB-MIMO achieves significantly lower computational complexity, 82%, 75%, and 67%, respectively. Additionally, as shown in Fig. 13, ASB-MIMO maintains comparable performance to AO-MIMO across various values of $N_t \times N_r$ and N.

VIII. COMPUTATIONAL COMPLEXITY ANALYSIS

In this section, we calculate the computational complexity of Algorithms 1, 2, and 3, as well as the ASB-MIMO and AO-MIMO schemes. Specifically, we first derive the complexity of each individual step within these algorithms. We then determine the total complexity by summing these steps and, where applicable, multiplying by the number of iterations required for convergence. Finally, we analyze the complexity gaps, which validates our empirical time complexity analysis.

TABLE 3. Computational complexity comparison of AO-MIMO and ASB-MIMO.

Algorithm	Symbol	Exact FLOPs per Operation	Iter.	Total Algorithm FLOPs
AO-MIMO	C_{init}	$16mN_tN_r$	No	$16mN_tN_r + i_{avg} \cdot [108m^3 + 16mN_tN_r + 8N_tN_r + N(8N_r + 8N_t + 10) + 6N_t + 2]$
	$C_\Phi + C_{\text{SVD}}$	$N(8N_r + 8N_t + 2) + 8N_tN_r + 6N_t - 1 + 16mN_tN_r$	Yes	
	C_{obj}	$8N + 3$	Yes	
ASB-MIMO	C_a	$16mN_tN_r + N(8N_r + 8N_t - 1)$	No	$32mN_tN_r + N(8N_tN_r + 22N_r + 8N_t + 14) + 7$
	C_b	$16mN_tN_r + N(8N_rN_t + 14N_r - 1)$	No	
	C_{select}	$16N + 7$	No	

A. COMPLEXITY ANALYSIS OF DIGITAL FILTERS

The transmit and receive digital filters, $\mathbf{w}_{k,l}$ and $\mathbf{f}_{k,l}$, are determined in (3) and (4) by solving the generalized eigenvalue problem for the matrix pair $(\mathbf{S}, \mathbf{T})$. Given that $\mathbf{S}$ and $\mathbf{T}$ are rank-1 matrices for all streams, we utilize the Lanczos algorithm to extract the dominant generalized eigenvector. This results in a computational complexity of $\mathcal{O}(mN_t)$ and $\mathcal{O}(mN_{r,k})$ respectively, where m denotes the number of Lanczos iterations.[2]

B. COMPLEXITY ANALYSIS OF POWER ALLOCATION

The power allocation subproblem (P1.3) is solved jointly over the power variables $\{p_{k,l}\}$ and auxiliary rate variables $\{\lambda_{k,l}\}$ using an interior-point method. The problem involves $N_{\text{var}} = 2\sum_k L_k$ optimization variables and $N_{\text{con}} = \sum_k L_k + K + 1$ constraints. Consequently, the computational complexity per iteration is $\mathcal{O}\left(\sqrt{N_{\text{con}}}N_{\text{var}}^3 \log(1/\varepsilon)\right)$. For a symmetric configuration where $L_k = L$ for all k, the complexity simplifies to $\mathcal{O}\left(K^{7/2}L^{7/2} \log(1/\varepsilon)\right)$, where $L = \min(N_t, N_r)$ [40]. This indicates that the power allocation overhead scales polynomially with the total number of spatial streams KL.

C. COMPLEXITY ANALYSIS OF USER GROUPING AND TOTAL OVERHEAD

The proposed user grouping (UG) strategies in (P1.9) and (P1.10) further mitigate complexity by restricting the RIS optimization to specific user subsets, denoted as $\mathcal{B}$ and $\mathcal{C}$. By substituting the global user set K with the reduced group sizes $|\mathcal{B} \cup \mathcal{C}|$ or $|\mathcal{B}|$, the dimension of the SDP subproblem is significantly lowered. The total complexity per outer iteration of Algorithm 1 is given by:

$$\mathcal{C}_{Total,Alg1} = I_{int}(\mathcal{C}_{filt} + \mathcal{C}_{\text{P1.3}}) + \mathcal{O}\left(\max\left\{\left(\sum_{k=1}^{K} L_k\right)^2, N\right\}^4 N^{1/2}\right), \quad (20)$$

where I_{int} is the number of internal iterations and $\mathcal{C}_{filt}$ represents the digital filter updates. For the UG-based Algorithms 2 and 3, the total complexity is reduced by replacing the global summation $\sum_{k=1}^{K} L_k$ with the group-specific summations $\sum_{k\in\mathcal{B}\cup\mathcal{C}} L_k$ and $\sum_{k\in\mathcal{B}} L_k$, respectively.

D. COMPUTATIONAL COMPLEXITY ANALYSIS FOR ASB-MIMO VERSUS AO-MIMO

In this section, we evaluate the computational efficiency of the proposed non-iterative ASB-MIMO algorithm compared to the benchmark AO-MIMO scheme. The complexity is measured in terms of total floating-point operations.

For the benchmark AO-MIMO, the total complexity C_{AO} scales linearly with the average number of iterations i_{avg} required for convergence, expressed as:

$$C_{\text{AO}} \approx C_{\text{init}} + i_{avg} \cdot (C_{\text{SVD},m} + C_\Phi + C_{\text{obj}}), \quad (21)$$

where C_{init} is the initial SVD cost ($108m^3$), $C_{\text{SVD},m}$ is the per-iteration beamforming update, C_Φ is the phase-shift optimization cost in (15), and C_{obj} is the cost of calculating the objective function for convergence checking.

In contrast, the proposed ASB-MIMO follows a deterministic approach. The total complexity C_{ASB} is given by:

$$C_{\text{ASB}} \approx C_a + C_b + C_{\text{select}}, \quad (22)$$

where C_a denotes the cost of calculating the first candidate set $(\mathbf{w}_a, \mathbf{f}_a, \mathfrak{z}_a)$, involving an SVD of $\mathbf{H}_d^H$ and a linear phase update. C_b represents the cost of the second candidate set $(\mathbf{w}_b, \mathbf{f}_b, \mathfrak{z}_b)$, which is dominated by the economy-size SVD of $\mathbf{G} \in \mathbb{C}^{N\times N_t}$ with complexity $\mathcal{O}(NN_t^2)$. Finally, C_{select} is the overhead of the performance-based selection step.

As demonstrated in Table 3, AO-MIMO incurs a significantly higher computational cost compared to the non-iterative ASB-MIMO. For example, for a 16 × 16 MIMO system with a typical profile of $i_{avg} = 2$ and $N = 50$, the proposed method achieves a complexity reduction of approximately 76.8%.

[2]Note that in our implementation, the MATLAB eig() function is used; the Lanczos bound represents the theoretical lower bound on this operation.

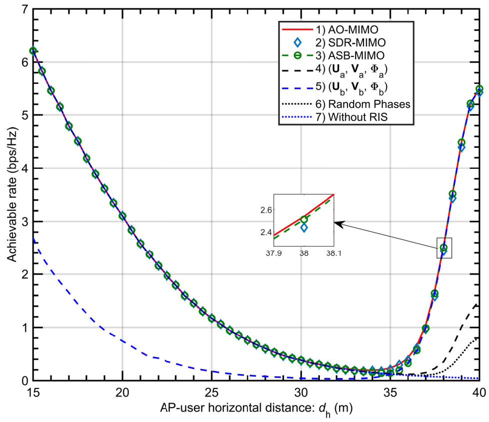

FIGURE 12. Achievable rate versus the AP-user horizontal distance for $N = 50$.

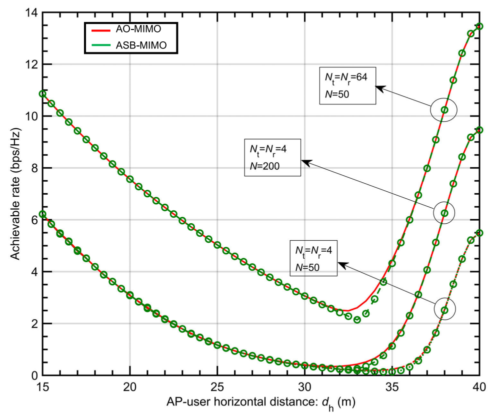

FIGURE 13. Achievable rate versus the AP-user horizontal distance for different $N_t \times N_r$ and N.

IX. DISCUSSION

Before concluding this paper, we highlight several important points below:

1) To demonstrate the benefits of the proposed user grouping (UG) methods, i.e., 3-UG and 2-UG in Algorithms 2 and 3, we used an SDR-based solution as a benchmark (Algorithm 1). However, the proposed UG methods are not limited to this benchmark; they can also be applied to other optimization techniques such as manifold optimization, gradient descent, semi-closed-form solutions, and deep learning methods. In particular, integrating UG methods prior to these algorithms can significantly reduce computational complexity without sacrificing the performance gains.
2) In this paper, we considered a simple RIS model, i.e., a metasurface with half-space reflective coverage. Nonetheless, the proposed UG and ASB methods are readily extendable to more advanced metasurface architectures, such as STAR-RISs [41], [42], [43], omni-RISs [44], and beyond-diagonal RISs [45].
3) Selection of the threshold τ for UG:
We discuss here an intuitive method to select the decision threshold τ for user grouping. The selection is motivated by the ASB framework. In the ASB scheme, when a user moves from the AP toward the RIS, the performance exhibits a characteristic performance switching behavior: system performance first decreases to a minimum point as the reflected channel starts to dominate, and then increases as the user approaches the RIS. This crossover point identifies the critical threshold for τ.
More specifically, for a given communication region and propagation environment, the threshold τ is determined from a single-user scenario as

$$\tau = \frac{\|\mathbf{H}_{r,k}^{H} 2 \mathbf{G}\|^2}{\|\mathbf{H}_{d,k}^{H}\|^2},$$

where 2 is the optimal RIS configuration for that single reference user, obtained in closed form via the ASB-MIMO rule of Section V. This calibration is performed once per deployment region and is therefore not part of the per-coherence-block computational budget.
Once τ is established, multiuser grouping is performed by calculating, for each user k, the ratio

$$\gamma_k = \frac{\|\mathbf{H}_{r,k}^{H} 2_k \mathbf{G}\|^2}{\|\mathbf{H}_{d,k}^{H}\|^2},$$

where 2_k denotes the single-user-optimal RIS configuration for user k, obtained in closed form via the ASB-MIMO rule applied to user k in isolation. Users are then assigned to groups by comparing γ_k to τ (and additionally to $\kappa\tau$ for the 3-UG case, as in Algorithm 2).
Computing 2_k at the grouping step requires one economy-size SVD of either $\mathbf{H}_{d,k}^{H}$ or $\mathbf{G}$ followed by a length-N phase update per user (cf. the ASB-MIMO entry of Table 3). The resulting per-coherence-block grouping overhead, $\mathcal{O}(K[N_t N_r m + N(N_r N_t + N_r + N_t)])$ FLOPs, is several orders of magnitude smaller than the SDP-based RIS optimization (P1.8) that the grouping removes for users in Group A; it is already included in the CPU running times of Table 1.
The numerical results in Fig. 9 provide clear evidence that this approach yields near-optimal performance across a wide range of user locations, validating the effectiveness of the proposed threshold-based grouping method.

X. CONCLUSION

This paper presents methods to significantly reduce the computational complexity of optimizing RIS phases.

First, we consider a RIS-assisted multiuser MIMO scenario and propose the 3-UG and 2-UG methods. These methods categorize users before performing RIS phase optimization. Specifically, in the 3-UG method (Algorithm 2), users are grouped into three categories, A, B, and C, based on a decision threshold, while the 2-UG method uses two categories. After grouping, we optimize the RIS phases only for Groups B and C in the 3-UG method, and only for Group B in the 2-UG method. Both methods achieve comparable performance to full optimization while offering substantial complexity reductions. For example, when $N_t = 64$, $K = 8$, and $N = 50$, the 3-UG and 2-UG methods achieve 75.12% and 73.26% reductions in complexity, respectively, with negligible performance loss.

Second, to further demonstrate the applicability of these methods, we consider a RIS-assisted multiuser scenario where each user is equipped with multiple receive antennas, enabling multiple data streams per user. In this context, the optimization problem involves a log-sum expression coupled with a discrete variable L_k, resulting in a mixed-integer optimization problem. We derive a convex formulation for L_k and propose a novel GM-based convex approximation for the log-sum expression. The proposed formulation reduces computational complexity by up to 70% compared to the standard log-sum formulation, while maintaining similar performance.

Third, we extend the UG concept to a RIS-assisted P2P MIMO scenario. Specifically, we derive two RIS phase configurations, each optimal in a different geographic region depending on the user's proximity to the AP or the RIS. The configuration with the stronger effective gain is selected adaptively. The proposed ASB-MIMO scheme is non-iterative, simple, and approximately 67%–85% less complex (depending on the MIMO size) than the most efficient existing benchmark. Due to its non-iterative nature and reliance on closed-form expressions, ASB-MIMO is a strong candidate for practical, real-time RIS-assisted MIMO systems.

Fourth, we propose a simple and intuitive method to select the threshold τ for user grouping, based on single-user performance behavior. This approach ensures near-optimal group assignments across multiuser scenarios while maintaining low computational complexity.

Finally, the proposed UG and ASB methods are not limited to conventional RISs. Their underlying principles are readily applicable to other architectures such as STAR-RISs, omni-RISs, and beyond-diagonal RISs.

REFERENCES

[1] M. A. ElMossallamy, H. Zhang, L. Song, K. G. Seddik, Z. Han, and G. Y. Li, "Reconfigurable intelligent surfaces for wireless communications: Principles, challenges, and opportunities," *IEEE Trans. Cognit. Commun. Netw.*, vol. 6, no. 3, pp. 990–1002, Sep. 2020.

[2] Q. Wu, S. Zhang, B. Zheng, C. You, and R. Zhang, "Intelligent reflecting surface-aided wireless communications: A tutorial," *IEEE Trans. Commun.*, vol. 69, no. 5, pp. 3313–3351, May 2021.

[3] X. Shao, C. You, and R. Zhang, "Intelligent reflecting surface aided wireless sensing: Applications and design issues," *IEEE Wireless Commun.*, vol. 31, no. 3, pp. 383–389, Jun. 2024.

[4] M. Munawar and K. Lee, "Dual-polarized IRS-assisted MIMO network," *IEEE Trans. Wireless Commun.*, vol. 23, no. 4, pp. 2519–2532, Apr. 2024.

[5] M. Munawar and K. Lee, "Power optimization of dual-polarized IRS-assisted wireless networks under spectral efficiency constraints," *IEEE Trans. Wireless Commun.*, vol. 24, no. 1, pp. 430–446, Jan. 2025.

[6] S. Sun, W. Jiang, S. Gong, and T. Hong, "Reconfigurable linear-to-linear polarization conversion metasurface based on PIN diodes," *IEEE Antennas Wireless Propag. Lett.*, vol. 17, no. 9, pp. 1722–1726, Sep. 2018.

[7] J. Wang, R. Yang, R. Ma, J. Tian, and W. Zhang, "Reconfigurable multifunctional metasurface for broadband polarization conversion and perfect absorption," *IEEE Access*, vol. 8, pp. 105815–105823, 2020.

[8] H. F. Ma, G. Z. Wang, G. S. Kong, and T. J. Cui, "Independent controls of differently-polarized reflected waves by anisotropic metasurfaces," *Sci. Rep.*, vol. 5, no. 1, p. 9605, Apr. 2015.

[9] Ö. Özdogan, E. Björnson, and E. G. Larsson, "Using intelligent reflecting surfaces for rank improvement in MIMO communications," in *Proc. IEEE Int. Conf. Acoust., Speech Signal Process. (ICASSP)*, May 2020, pp. 9160–9164.

[10] F. Xu, J. Yao, W. Lai, K. Shen, X. Li, X. Chen, and Z.-Q. Luo, "Blind beamforming for coverage enhancement with intelligent reflecting surface," *IEEE Trans. Wireless Commun.*, vol. 23, no. 11, pp. 15736–15752, Nov. 2024.

[11] M. Cui, G. Zhang, and R. Zhang, "Secure wireless communication via intelligent reflecting surface," *IEEE Wireless Commun. Lett.*, vol. 8, no. 5, pp. 1410–1414, Oct. 2019.

[12] Q. Wu and R. Zhang, "Beamforming optimization for wireless network aided by intelligent reflecting surface with discrete phase shifts," *IEEE Trans. Commun.*, vol. 68, no. 3, pp. 1838–1851, Mar. 2020.

[13] M. Munawar and K. Lee, "Dual-polarized IRS-assisted wireless network: Relative phase modulation," *EURASIP J. Wireless Commun. Netw.*, vol. 2024, no. 1, p. 22, May 2024.

[14] S. Lin, B. Zheng, G. C. Alexandropoulos, M. Wen, M. D. Renzo, and F. Chen, "Reconfigurable intelligent surfaces with reflection pattern modulation: Beamforming design and performance analysis," *IEEE Trans. Wireless Commun.*, vol. 20, no. 2, pp. 741–754, Feb. 2021.

[15] B. Zheng, C. You, W. Mei, and R. Zhang, "A survey on channel estimation and practical passive beamforming design for intelligent reflecting surface aided wireless communications," *IEEE Commun. Surv. Tut.*, vol. 24, no. 2, pp. 1035–1071, 2nd Quart., 2022.

[16] A. Tishchenko, M. Khalily, A. Shojaeifard, F. Burton, E. Björnson, M. Di Renzo, and R. Tafazolli, "The emergence of multi-functional and hybrid reconfigurable intelligent surfaces for integrated sensing and communications—A survey," *IEEE Commun. Surv. Tut.*, vol. 27, no. 5, pp. 2895–2936, Oct. 2025.

[17] S. Hassouna, M. A. Jamshed, J. Rains, J. u. R. Kazim, M. U. Rehman, M. Abualhayja, L. Mohjazi, T. J. Cui, M. A. Imran, and Q. H. Abbasi, "A survey on reconfigurable intelligent surfaces: Wireless communication perspective," *IET Commun.*, vol. 17, no. 5, pp. 497–537, 2023.

[18] A. Umer, I. Müürsepp, M. M. Alam, and H. Wymeersch, "Reconfigurable intelligent surfaces in 6G radio localization: A survey of recent developments, opportunities, and challenges," *IEEE Commun. Surv. Tuts.*, vol. 27, no. 6, pp. 3526–3560, Dec. 2025.

[19] M. Munawar and K. Lee, "Low-complexity adaptive selection beamforming for IRS-assisted single-user wireless networks," *IEEE Trans. Veh. Technol.*, vol. 72, no. 4, pp. 5458–5462, Apr. 2023.

[20] D. Li, "Fairness-aware multiuser scheduling for finite-resolution intelligent reflecting surface-assisted communication," *IEEE Commun. Lett.*, vol. 25, no. 7, pp. 2395–2399, Jul. 2021.

[21] M. Hua, Q. Wu, W. Chen, O. A. Dobre, and A. L. Swindlehurst, "Secure intelligent reflecting surface-aided integrated sensing and communication," *IEEE Trans. Wireless Commun.*, vol. 23, no. 1, pp. 575–591, Jan. 2024.

[22] Z. Luo, W. Ma, A. M. So, Y. Ye, and S. Zhang, "Semidefinite relaxation of quadratic optimization problems," *IEEE Signal Process. Mag.*, vol. 27, no. 3, pp. 20–34, May 2010.

[23] J. Hu, X. Liu, Z.-W. Wen, and Y.-X. Yuan, "A brief introduction to manifold optimization," *J. Oper. Res. Soc. China*, vol. 8, no. 2, pp. 199–248, Jun. 2020.

[24] S. Ruder, "An overview of gradient descent optimization algorithms," 2016, *arXiv:1609.04747*.

[25] M. Kojima and L. Tunçel, "Cones of matrices and successive convex relaxations of nonconvex sets," *SIAM J. Optim.*, vol. 10, no. 3, pp. 750–778, Jan. 2000.

[26] S. Kimaryo and K. Lee, "Low-complexity IRS beamforming based on sphere decoding and Tabu search," *J. Commun. Netw.*, vol. 25, no. 3, pp. 299–311, Jun. 2023.
[27] E. Zafra, S. Vazquez, A. M. Alcaide, L. G. Franquelo, J. I. Leon, and E. P. Martin, "K-best sphere decoding algorithm for long prediction horizon FCS-MPC," *IEEE Trans. Ind. Electron.*, vol. 69, no. 8, pp. 7571–7581, Aug. 2022.
[28] Q. Wu and R. Zhang, "Intelligent reflecting surface enhanced wireless network via joint active and passive beamforming," *IEEE Trans. Wireless Commun.*, vol. 18, no. 11, pp. 5394–5409, Nov. 2019.
[29] S. Zhang and R. Zhang, "Capacity characterization for intelligent reflecting surface aided MIMO communication," *IEEE J. Sel. Areas Commun.*, vol. 38, no. 8, pp. 1823–1838, Aug. 2020.
[30] X. Chen, J. C. Ke, W. Tang, M. Z. Chen, J. Y. Dai, E. Basar, S. Jin, Q. Cheng, and T. J. Cui, "Design and implementation of MIMO transmission based on dual-polarized reconfigurable intelligent surface," *IEEE Wireless Commun. Lett.*, vol. 10, no. 10, pp. 2155–2159, Oct. 2021.
[31] R. Fara, P. Ratajczak, D.-T. Phan-Huy, A. Ourir, M. Di Renzo, and J. de Rosny, "A prototype of reconfigurable intelligent surface with continuous control of the reflection phase," *IEEE Wireless Commun.*, vol. 29, no. 1, pp. 70–77, Feb. 2022.
[32] Y. Liu, X. Mu, J. Xu, R. Schober, Y. Hao, H. V. Poor, and L. Hanzo, "STAR: Simultaneous transmission and reflection for 360° coverage by intelligent surfaces," *IEEE Wireless Commun.*, vol. 28, no. 6, pp. 102–109, Dec. 2021.
[33] H. Zhang and B. Di, "Intelligent omni-surfaces: Simultaneous refraction and reflection for full-dimensional wireless communications," *IEEE Commun. Surv. Tut.*, vol. 24, no. 4, pp. 1997–2028, 4th Quart., 2022.
[34] D. Mishra and H. Johansson, "Channel estimation and low-complexity beamforming design for passive intelligent surface assisted MISO wireless energy transfer," in *Proc. IEEE Int. Conf. Acoust., Speech Signal Process. (ICASSP)*, May 2019, pp. 4659–4663.
[35] X. Ma, Z. Chen, W. Chen, Z. Li, Y. Chi, C. Han, and S. Li, "Joint channel estimation and data rate maximization for intelligent reflecting surface assisted terahertz MIMO communication systems," *IEEE Access*, vol. 8, pp. 99565–99581, 2020.
[36] Z. Wang, L. Liu, and S. Cui, "Channel estimation for intelligent reflecting surface assisted multiuser communications: Framework, algorithms, and analysis," *IEEE Trans. Wireless Commun.*, vol. 19, no. 10, pp. 6607–6620, Oct. 2020.
[37] K. Shen and W. Yu, "Fractional programming for communication systems—Part I: Power control and beamforming," *IEEE Trans. Signal Process.*, vol. 66, no. 10, pp. 2616–2630, May 2018.
[38] M. Grant and S. Boyd. *CVX: MATLAB Software for Disciplined Convex Programming*. Accessed: Sep. 2024. [Online]. Available: http://cvxr.com/cvx.
[39] Z. Zhang, L. Dai, X. Chen, C. Liu, F. Yang, R. Schober, and H. V. Poor, "Active RIS vs. passive RIS: Which will prevail in 6G?" *IEEE Trans. Commun.*, vol. 71, no. 3, pp. 1707–1725, Mar. 2023.
[40] C. Helmberg, F. Rendl, R. J. Vanderbei, and H. Wolkowicz, "An interior-point method for semidefinite programming," *SIAM J. Optim.*, vol. 6, no. 2, pp. 342–361, 1996.
[41] S. Ahmed, A. E. Kamal, M. Y. Selim, M. A. Hossain, and S. R. Sabuj, "Optimizing small cell performance: A new MIMO paradigm with distributed ASTAR-RISs," *IEEE Open J. Veh. Technol.*, vol. 6, pp. 128–144, 2024.
[42] X. Li, J. Zhao, G. Chen, W. Hao, D. B. D. Costa, A. Nallanathan, H. Shin, and C. Yuen, "STAR-RIS-assisted covert wireless communications with randomly distributed blockages," *IEEE Trans. Wireless Commun.*, vol. 24, no. 6, pp. 4690–4705, Jun. 2025.
[43] I. F. Mendes, D. L. F. Duarte, L. G. B. Guedes, L. S. Souza, R. S. Silva, V. D. P. Souto, and R. D. Souza, "A survey on federated learning in RIS, STAR-RIS, and BD-RIS-assisted wireless networks," *IEEE Open J. Commun. Soc.*, vol. 7, pp. 1654–1698, 2026.
[44] M. Hou, Y. Qin, J. Chen, L. Zhang, L. Song, and S. Gao, "A multi-dimensional multiplexing intelligent omni-surface: Principles and experiments," *IEEE Wireless Commun.*, pp. 1–9, Jan. 2026.
[45] W. Ullah Khan, M. Ahmed, C. Kumar Sheemar, M. Di Renzo, E. Lagunas, A. Mahmood, S. Tariq Shah, O. A. Dobre, J. Querol, and S. Chatzinotas, "Survey on beyond diagonal RIS enabled 6G wireless networks: Fundamentals, recent advances, and challenges," 2025, *arXiv:2503.08423*.

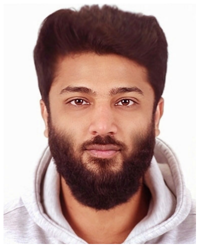

MUTEEN MUNAWAR (Student Member, IEEE) received the B.Sc. and M.Sc. degrees in electrical engineering, in 2019 and 2021, respectively, and the second master's degree in electrical and information engineering from Seoul National University of Science and Technology, South Korea. He is currently pursuing the Ph.D. degree with UGent, Belgium. He was with the Communication and Signal Processing Laboratory, South Korea, from February 2023 to September 2023. He is with IMEC, Leuven, as a Researcher. His research interests include wireless communications, applied machine learning, and digital multipliers. He received the Best Project Award at the IEEE Riphah Innovation Summit (IRIS), in 2019.

MAMOUN GUENACH (Senior Member, IEEE) received the degree from EMI, Morocco, in 1995, and the Ph.D. degree from UCL, Belgium, in 2002. He was a Postdoctoral Researcher with Ghent University, from 2002 to 2006, where he has been a part-time Visiting Research Professor, since 2015. He was a member of Nokia Bell Labs Technical Staff, from 2006 to 2019. Since 2019, he has been with IMEC, Leuven, as a Research Scientist. His main research interests include coding, modulation, synchronization, and MIMO equalization for high-speed wired and wireless communication technologies.

INGRID MOERMAN (Fellow, IEEE) received the degree in electrical engineering and the Ph.D. degree from Ghent University, in 1987 and 1992, respectively. She became a part-time Professor with Ghent University, in 2000. She is currently a Staff Member with IDLab, a core research group of IMEC, with research activities embedded at Ghent University and the University of Antwerp. She coordinates the research activities on intelligent wireless networking (iWiNe) with Ghent University, where she leads a team of more than 30 researchers. She is also the Program Manager of the Deterministic Networking track, part of the Connectivity Program, IMEC. In this role, she coordinates research on end-to-end wired/wireless networking solutions for business and mission-critical applications that must meet strict quality of service requirements in terms of throughput, bounded latency, and reliability in private wireless environments. She has extensive experience in running and coordinating national and EU research-funded projects.